iScience

CellPress
OPEN ACCESS

Article

Developmentally Regulated Novel Non-coding Anti-sense Regulators of mRNA Translation in *Trypanosoma brucei*

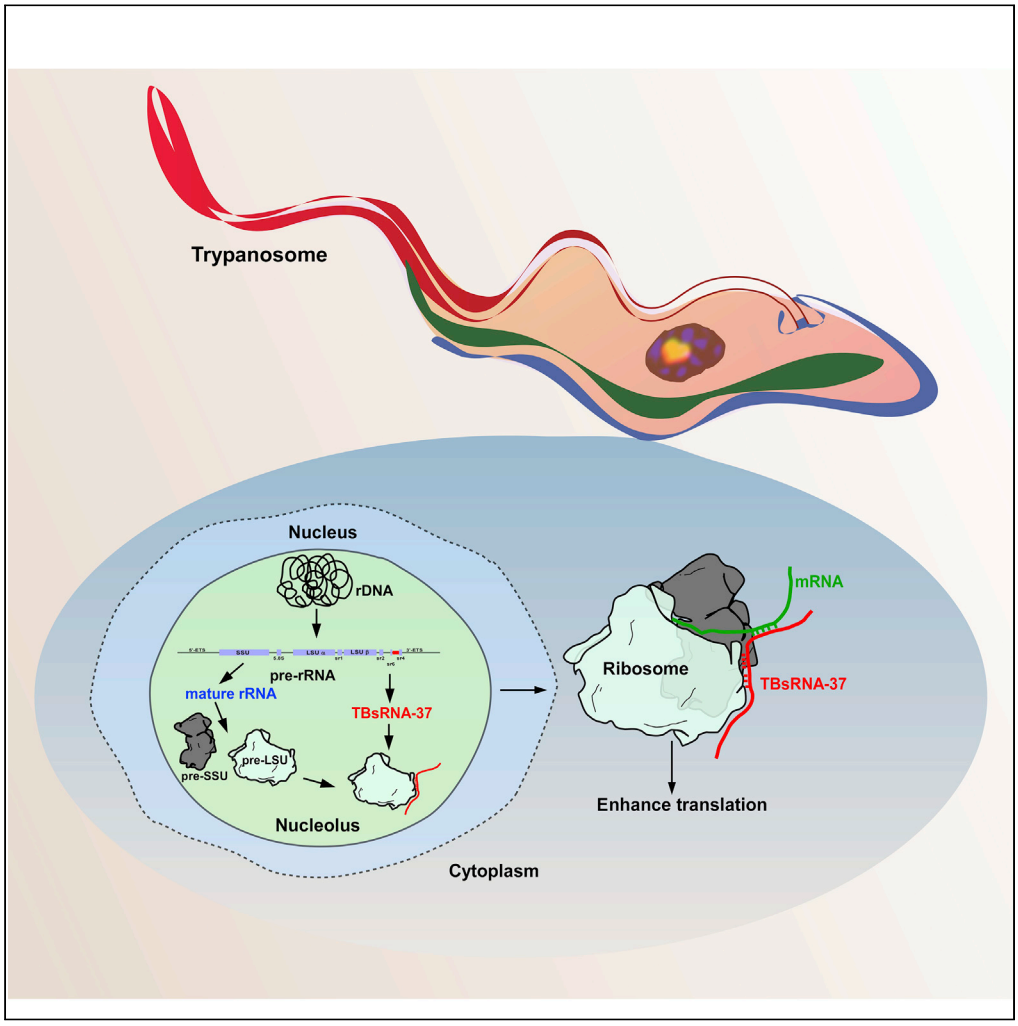

K. Shanmugha Rajan, Tirza Doniger, Smadar Cohen-Chalamish, ..., Ron Unger, Christian Tschudi, Shulamit Michaeli

shulamit.michaeli@biu.ac.il

HIGHLIGHTS

Trypanosome non-coding RNAs (ncRNAs) are developmentally regulated during cycling between two hosts

ncRNAs originate from rRNA locus and associate with the ribosome *en route* to cytoplasm

In vivo cross-linking enable identification of target RNA species regulated by ncRNAs

Trypanosomes possess anti-sense ncRNAs that regulate translation

Rajan et al., iScience *23*, 101780
December 18, 2020
https://doi.org/10.1016/j.isci.2020.101780

iScience

CellPress
OPEN ACCESS

Article

Developmentally Regulated Novel Non-coding Anti-sense Regulators of mRNA Translation in *Trypanosoma brucei*

K. Shanmugha Rajan,[1] Tirza Doniger,[1] Smadar Cohen-Chalamish,[1] Praveenkumar Rengaraj,[1] Beathrice Galili,[1] Saurav Aryal,[1] Ron Unger,[1] Christian Tschudi,[2] and Shulamit Michaeli[1,3,*]

SUMMARY

The parasite *Trypanosoma brucei* is the causative agent of sleeping sickness and cycles between insect and mammalian hosts. The parasite appears to lack conventional transcriptional regulation of protein coding genes, and mRNAs are processed from polycistronic transcripts by the concerted action of *trans*-splicing and polyadenylation. Regulation of mRNA function is mediated mainly by RNA binding proteins affecting mRNA stability and translation. In this study, we describe the identification of 62 non-coding (nc) RNAs that are developmentally regulated and/or respond to stress. We characterized two novel anti-sense RNA regulators (TBsRNA-33 and 37) that originate from the rRNA loci, associate with ribosomes and polyribosomes, and interact *in vivo* with distinct mRNA species to regulate translation. Thus, this study suggests for the first-time anti-sense RNA regulators as an additional layer for controlling gene expression in these parasites.

INTRODUCTION

In eukaryotes, non-coding RNAs (ncRNAs) are classified as small (below 200 nt) or long ncRNAs, where the latter harbor a 5′-cap and are polyadenylated (Hombach and Kretz, 2016). The small ncRNAs include RNAs involved in splicing, such as U snRNAs, small nucleolar RNAs (snoRNAs) involved in rRNA processing and modification, 7SL RNA (the signal recognition particle RNA), telomerase RNA, and others (Morris and Mattick, 2014). The best studied small ncRNAs are microRNAs and siRNAs, which are processed by DICER and bind ARGONAUTE (Wilson and Doudna, 2013). MicroRNAs bind to the 3′ UTR by base-pairing, and regulate both mRNA stability and translation (Mohr and Mott, 2015). In prokaryotes, small RNAs utilize anti-sense mechanisms to regulate mRNA function under stress, following metabolic changes, and to control virulence, and they affect translation and/or stability, together with the binding protein Hfq (Wagner and Romby, 2015).

Trypanosoma brucei is the causative agent of sleeping sickness and cycles between two hosts. In the tsetse fly, the parasite propagates in the midgut in the procyclic stage (PCF), and in the mammalian host it transforms to the bloodstream form (BSF) (Rodrigues et al., 2014). These organisms lack conventional promoters for genes encoding mRNA (Clayton, 2016), and mRNAs are transcribed as long polycistronic transcripts that are processed by concerted action of *trans*-splicing and polyadenylation (Michaeli, 2011). Post-transcriptional regulation is mainly achieved by RNA binding proteins (RBPs), which regulate mRNA stability and translation and control gene expression under stress and during the developmental cycle (Clayton, 2013). For instance, overexpression of a single RBP in PCF, such as RBP6 or RBP10, induces transformation to a form that can initiate infection in the mammalian host (Kolev et al., 2012; Mugo and Clayton, 2017). The reprogramming of gene expression during cycling between the two hosts involves changes in mRNA abundance and in the proteome (Butter et al., 2013; Naguleswaran et al., 2018; Queiroz et al., 2009). Ribosome profiling of the two life stages revealed that thousands of genes show changes in protein synthesis mediated by both mRNA abundance and translational efficiency (Jensen et al., 2014).

Trypanosomes possess all the conventional eukaryotic small RNA types such as U snRNAs (Liang et al., 2003; Rajan et al., 2019a, 2019b), snoRNAs (Chikne et al, 2016, 2019; Michaeli et al., 2012; Rajan et al., 2020), telomerase RNA (Gupta et al., 2013a; Sandhu et al., 2013), 7SL RNA (Michaeli, 2014), and Vault

[1]The Mina and Everard Goodman Faculty of Life Sciences and Advanced Materials and Nanotechnology Institute, Bar-Ilan University, Ramat-Gan 52900, Israel

[2]Department of Epidemiology of Microbial Diseases, Yale School of Public Health, New Haven, CT 06536, USA

[3]Lead Contact

*Correspondence: shulamit.michaeli@biu.ac.il

https://doi.org/10.1016/j.isci.2020.101780

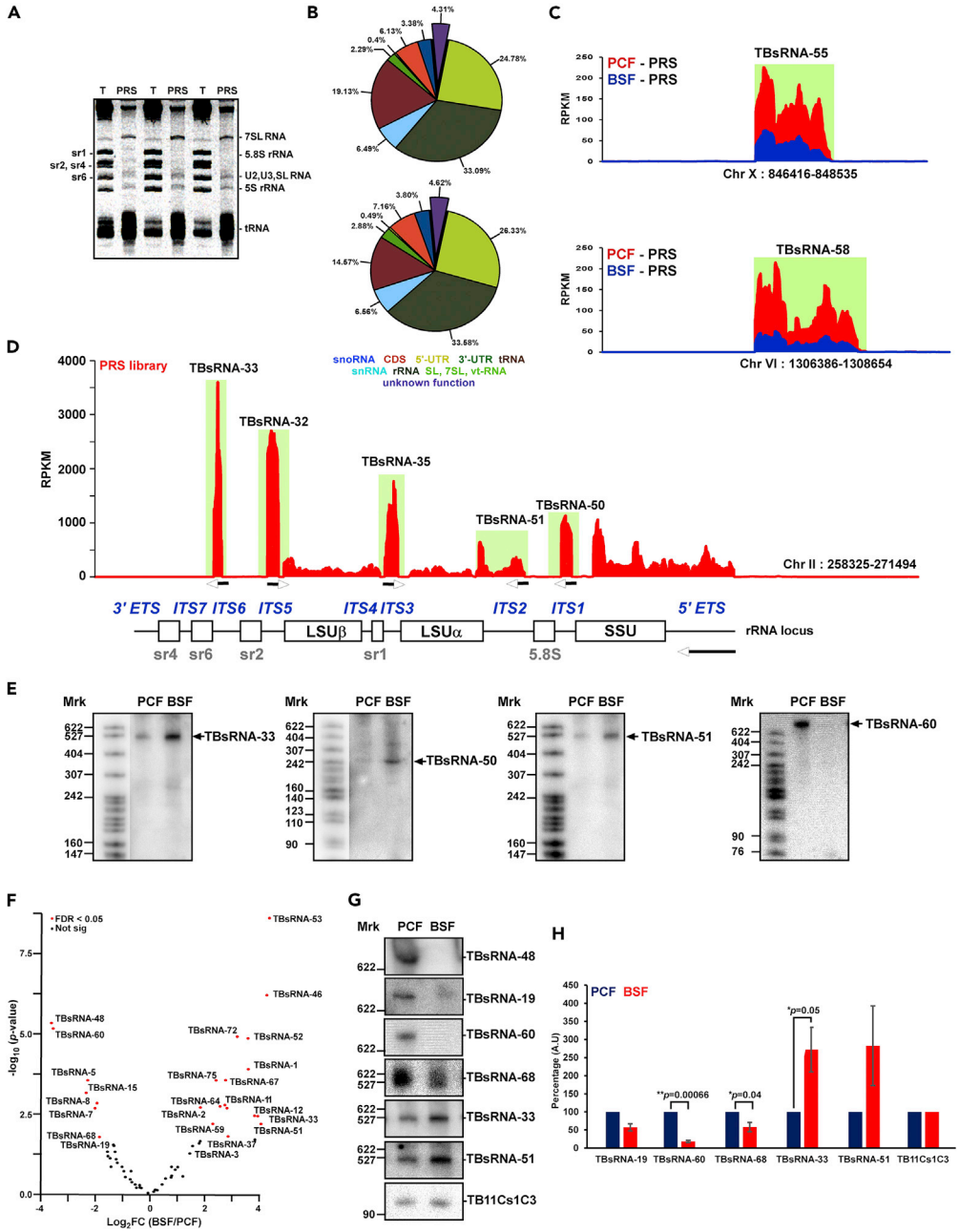

Figure 1. TBsRNAs Are Developmentally Regulated

(A) Enrichment of ncRNAs from *T. brucei* cell extracts. Whole cell extracts from 2 × 10^9 cells were prepared and depleted of ribosomes, as described in (Chikne et al., 2016; Rajan et al., 2019a, 2019b). RNA was extracted from PRS and total cell lysate (T), separated on a 10% denaturing gel, and stained with ethidium bromide.

(B) Example of the RNA composition of the PRS library. Pie diagram depicts the relative abundance of various ncRNA types in two libraries. Approximately, 13 different PRS libraries were used to validate the existence of the 62 ncRNA described in this study.

(C) Representative snapshot coverage of two novel TBsRNAs on their corresponding chromosome locus, given in RPKM.

(D) Distribution of the ncRNA reads across the pre-rRNA given in Reads per kilobase per million (RPKM). The arrows indicate the direction of transcription. The domains of the pre-rRNA are indicated.

(E) Northern analysis of ncRNAs. Total *T. brucei* RNA (20μg) was separated on denaturing gels and probed with ^{32}P-labeled anti-sense RNA probe. ^{32}P-labeled pBR322 DNA *MspI* digest was used as a size marker.

Figure 1. *Continued*

(F) TBsRNAs are developmentally regulated. The volcano plot was generated by DESeq2 (Anders and Huber, 2010) using three independent replicates of PRS RNA libraries of both PCF and BSF for the TBsRNA population. TBsRNAs that are developmentally regulated (FDR<0.05, and FC > 2) are indicated in red.

(G) TBsRNA expression analysis. Total RNA (20 μg) from PCF or BSF was separated on a 6% or 10% denaturing polyacrylamide gel and subjected to Northern analysis using anti-sense RNA probes to TBsRNA.

(H) Quantification of TBsRNA expression level based on Northern analysis. Expression data are presented as mean ± S.E.M. Experiments were done in triplicate (n = 3). TB11Cs1C3 was used as loading control. All densitometry data used in this figure were calculated by ImageJ (https://imagej.nih.gov/ij/) software.

RNA (Kolev et al., 2019). Surprisingly, trypanosomes possess almost double the number of snoRNAs compared to yeast, which have a similar genome-size (Rajan et al., 2019a, 2019b). Pseudouridines guided by H/ACA snoRNAs, are developmentally regulated, with higher levels in the BSF, enabling the parasite to cope with the temperature shift while cycling between the hosts (Chikne et al., 2016). The number of 2′-*O*-methylations guided by C/D snoRNAs is exceptionally large (~100) and these modifications are also developmentally regulated but to a lesser extent (Rajan et al., 2020). At least 20 snoRNAs are involved in the complex rRNA processing necessary for forming the fragmented large subunit rRNA (LSU) that is composed of two large molecules and four small ones, termed small rRNA (srRNA or sr) (Chikne et al., 2019).

We previously described the identification of small RNAs enriched by fractionation of RNA protein complexes, which led to the identification of small RNA molecules (TBsRNAs) (Michaeli et al., 2012). The most abundant small RNAs in trypanosomes are siRNAs derived from the retroposon families and from centromeric repeats, but no evidence exists for the presence of canonical microRNAs (miRNAs) bound to the ARGONAUTE protein (Tschudi et al., 2012).

Here, we report the identification of novel ncRNAs that were enriched and sequenced upon removal of ribosomes. Among the 62 ncRNA molecules described, we identified 22 ncRNAs that are developmentally regulated in the two life stages, as well as ncRNAs that change in abundance following stress. We utilized an *in vivo* UV cross-linking-ligation approach to identify the targets of these ncRNAs, and focused our functional studies on TBsRNA-33 and 37. These RNAs are processed from the internal transcribed spacer (ITS) of pre-rRNA, and appear to move with the ribosomes to the cytoplasm where these interact with distinct subset of mRNAs. We show that the ncRNA can repress/enhance the synthesis of the protein encoded by target mRNAs. This is the first report of a stable anti-sense regulator in trypanosomes that participate in regulating stage-specific gene expression.

RESULTS

Identification of Developmentally Regulated ncRNAs

To explore the constellation of ncRNAs in trypanosomes and search for anti-sense regulators, we analyzed by RNA-seq the repertoire of ncRNAs enriched in post-ribosomal supernatant (PRS) (Figure 1A). Total cell lysate was prepared, RNPs were extracted with 300mM KCl, and the ribosomes were removed by ultracentrifugation. RNA from the PRS was used to prepare RNA-seq libraries from both PCF and BSF, as previously described (Chikne et al., 2016; Rajan et al., 2019a, 2019b, 2020). The libraries contained the entire population of ncRNAs (U snRNA, snoRNAs, 7SL RNA, Vault RNA, and tRNAs, Figure 1B) but also ~62 relatively abundant RNAs with unknown function (Data S1, S2, and S3). The list of these RNAs (Data S2) and their chromosomal location (Data S3) are presented. By inspecting the chromosomal location of these ncRNAs by IGV viewer (Robinson et al., 2011), we found that most of these ncRNAs were located in intergenic regions (Figure 1C) and 3′ UTRs of mRNAs; to our surprise, we also found that five ncRNAs were localized in the ITS, and one in the external transcribed spacer of pre-rRNA (Figure 1D). Four ncRNAs, including TBsRNA-33, are derived from the pre-RNA precursor, but two ncRNAs, TBsRNA-32 and 35, are transcribed from the opposite strand (Figures 1D and 1E), likely by polymerase III, as these are enriched in the ChIP-seq with polymerase III tagged protein (Kolev et al., 2019).

Next, we used RNA-seq to examine the expression of a subset of ncRNAs in the two life stages and found 22 developmentally regulated ncRNAs that are preferentially expressed in either the PCF or BSF (Table S1, Figures 1F–1H). DESeq2 (Anders and Huber, 2010) analysis of the TBsRNA population suggested that 15 ncRNAs are upregulated in the BSF, and 7 ncRNAs are downregulated in this form (Tables S1 and S2). Note that among the ncRNAs identified are RNAs ranging from ~90 to 500 nt in length (Tables S1 and

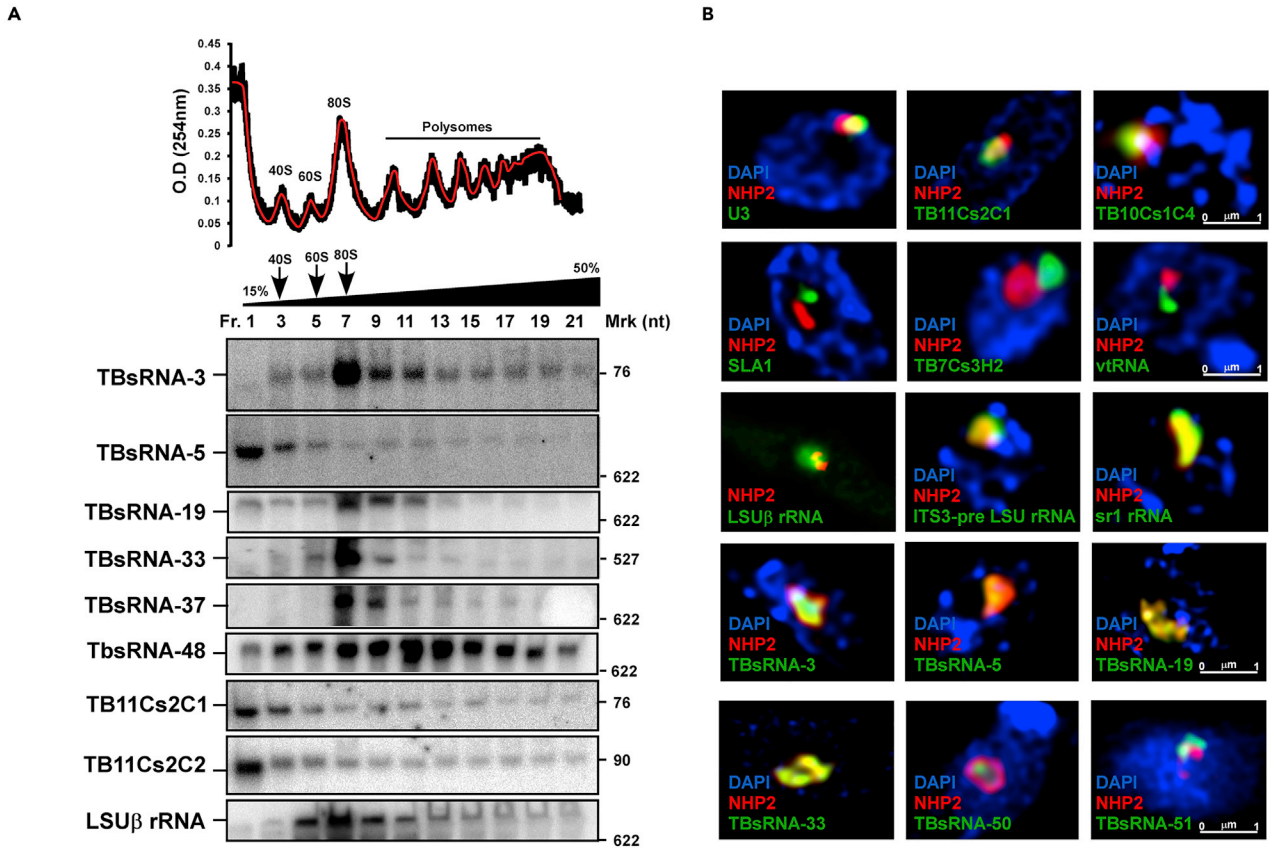

Figure 2. Localization of TBsRNAs

(A) Fractionation of TBsRNA. Whole cell extract from procyclic cells (2×10^9) was fractionated on (15–50%) sucrose gradient at 70,000 rpm for 1.5 hr using a Beckman SW41 rotor. 400 μL fractions were collected using the ISCO gradient fractionation system. The fractions were deproteinized and the RNA was separated on a 6% or 10% polyacrylamide-denaturing gel and subjected to Northern analysis using anti-sense RNA probes hybridizing to TBsRNAs, as indicated. The optical density of the fractions is presented.

(B) High-resolution fluorescence *in situ* hybridization coupled with immunofluorescence was performed for the indicated RNAs (green) and NHP2 (red). DNA was stained with DAPI (blue). The scale bar is indicated.

S2) and vary in abundance. The most abundant ncRNAs are TBsRNA-32 and TBsRNA-49 (Tables S1 and S2). The relative expression was confirmed for a subset of ncRNAs by Northern analysis (three replicates) supporting the PRS RNA-seq data (Figures 1F–1H). The quantification of the expression data based on Northern analyses verified distinct ncRNAs that are differentially expressed ($p < 0.05$) between the two stages (Figures 1G and 1H).

Nuclear Localization and Association of the Novel ncRNAs with RNPs

As a first step toward exploring the function of the novel ncRNAs, their association with other RNPs was examined. Two major types of RNPs greater than 80S were described in trypanosomes: polyribosomes and the processome involved in rRNA processing (Rajan et al., 2019a, 2019b). To this end, whole cell extracts were fractionated on 15–45% sucrose gradients, and the RNA was subjected to Northern analysis with gene-specific probes. The results (Figure 2A) indicate that the ncRNAs can be categorized to two groups. One group of ncRNAs are found in small RNPs (peak found in fractions 1–3) that also associate with larger RNP complexes such as the C/D snoRNAs TB11Cs2C2 and C1, which were shown to participate in rRNA processing (Gupta et al., 2010). Indeed, the ncRNA TBsRNA-5 fractionated similarly to C/D snoRNAs involved in rRNA processing (TB11Cs2C2 and C1). However, this RNA lacks the boxes specifying C/D or H/ACA families and therefore is not a member of these families. Interestingly, this RNA is localized in the center of the nucleolus and is not found in all domains containing the NHP2 protein, which is the core protein of the H/ACA RNA (Barth et al., 2005) (Figures 2B and S1). This localization differs from that of U3 involved in SSU processing (Hartshorne and Agabian, 1993), since U3 is not found in the center of the

nucleolus. Its possible role in rRNA processing will require further experimentation. Members of the second group (TBsRNA-3, TBsRNA-19, TBsRNA-33, TBsRNA-37) are not present in small distinct RNPs (like TB11Cs2C1, and C2) and their major peak is associated with the 80S ribosomes. The rest of the hybridization signal is distributed on polyribosomes. In the nucleolus, these RNAs are co-localized with NHP2 (Figures 2B and S1). This distribution is distinct from those RNAs involved in rRNA processing and those that guide the modification on snRNAs, such as the spliced leader associated RNA (SLA1), which guides Ψ on SL RNA (Liang et al., 2002), and TB7Cs3H2, which guides Ψ on rRNA and U2 snRNA (Rajan et al., 2019a, 2019b), as well as vault RNA (vtRNA) which we showed recently to affect the *trans*-splicing process (Kolev et al., 2019) (Figures 2B and S1). Despite the fact that TBsRNA-33 and 37 clearly fractionate with the 80S ribosomes and polysomes, these ncRNAs could not be detected by *in situ* hybridization in the cytoplasm due to their low abundance compared to rRNA (Figures 2B and S1), which has a dispersed pattern in the cytoplasm and gives a weaker signal compared to the foci in the nucleolus.

"Tell Me Who You Interact with and I Will Tell You Who You Are" mRNAs Associated with Distinct ncRNAs

The presence of ncRNAs on 80S ribosomes and polysomes led us to investigate whether these ncRNAs interact with distinct mRNAs to regulate their fate. We employed the methodology recently implemented by us to investigate the small RNA interactome of *T. brucei* using *in vivo* cross-linking (Rajan et al., 2019a, 2019b), as depicted in (Figure 3A). The method involves *in vivo* cross-linking in the presence of psoralen, which increases the efficacy of cross-linking by ten-fold (Garrett-Wheeler et al., 1984), preparation of PRS extracts, extracting the RNA, ligating the interacting RNA, and preparing RNA-seq libraries to detect the chimeric RNA products including the ncRNA and its interacting mRNA (Figure 3A). UV cross-linking enriched for such chimeric RNAs and chimera production was dependent on ligation and increased the detection of intermolecular interactions (Figure 3B) (Table S3). For instance, both U4/U6 and U6/U2 chimeras were highly enriched, as presented by the number of chimeric RNAs detected following ligation. The interactions are also depicted in a Circos plot (Figure 3C). As an example, for the specificity of the method, the chimera generated between the C/D snoRNA TB10Cs1C4 and its rRNA target is shown in Figure 3D. The distribution of the chimeric RNA reads on pre-rRNA indicated that the peak of ligated RNA was found around the interaction domain between the C/D snoRNA and rRNA, guiding 2′-*O* methylation at Gm552 (Figure 3D). Additional examples are presented in Figure S2, also demonstrating that the peak for the chimeric snoRNA/rRNA is always in the vicinity of the 10–21 bp duplex that is formed between the C/D snoRNA and its rRNA target. The chimeric RNA sequence generated between TB10Cs1C4 and rRNA is presented, demonstrating that the chimeric molecules were generated by ligation within the interaction domain or in its vicinity (Figure 3D). Note that although most of the ligated molecules generated by the cross-linking of the snoRNAs with its target were within the interaction domain, ligations also took place with domains that are as far as ~400 nt away from the interaction region. Thus, the putative interaction domain can be mapped to the region where most of the chimeric reads were derived, as is generally the case with abundant classes of ncRNA, such as snoRNAs. However, this method cannot unequivocally provide base pair resolution of the interaction domain, as many of the chimeras generated contain regions that are distant from the interaction site.

Based on the evidence that this method can identify ncRNA-target interactions, the interaction between the ncRNA and mRNAs was explored in the libraries (Figure 4A). We inspected six libraries specified in Figure 4A, showing that ~267 mRNAs were cross-linked to 62 ncRNAs (Figure 4A). Note that variation exists in the abundance of chimeric molecules detected in the PRS due to differences in the efficiency of extraction of the RNAs from the different RNPs. The PRS extraction enriches for the ncRNAs and enables the detection of their corresponding targets. To obtain independent evidence for the interactions leading to the formation of the chimeric molecules *in vivo*, we attempted a reverse experiment, in which we enriched these chimeric molecules by selecting the target mRNA. To this end, cells were treated with AMT psoralen, cross-linked, RNA was extracted with Trizol, and mRNAs were enriched with oligo (dT). After mild alkaline hydrolysis to randomly cleave the mRNA and ncRNA, the cross-linked molecules were ligated, and the cross-linked adducts were released by reversal of cross-linking prior to library preparation. Indeed, 200 potential TBsRNA-mRNA interactions were identified in both these libraries (Table S4, Data S4), suggesting that these reflect genuine *in vivo* interactions. To control for the specificity of the protocol, we performed a parallel experiment including all steps except the ligation between the RNA molecules, and prepared libraries for RNA-seq. Species that appeared in both PRS and poly(A) selected interactome libraries were considered potential chimeric molecules. In addition, valid chimera was required to be at least 3-fold

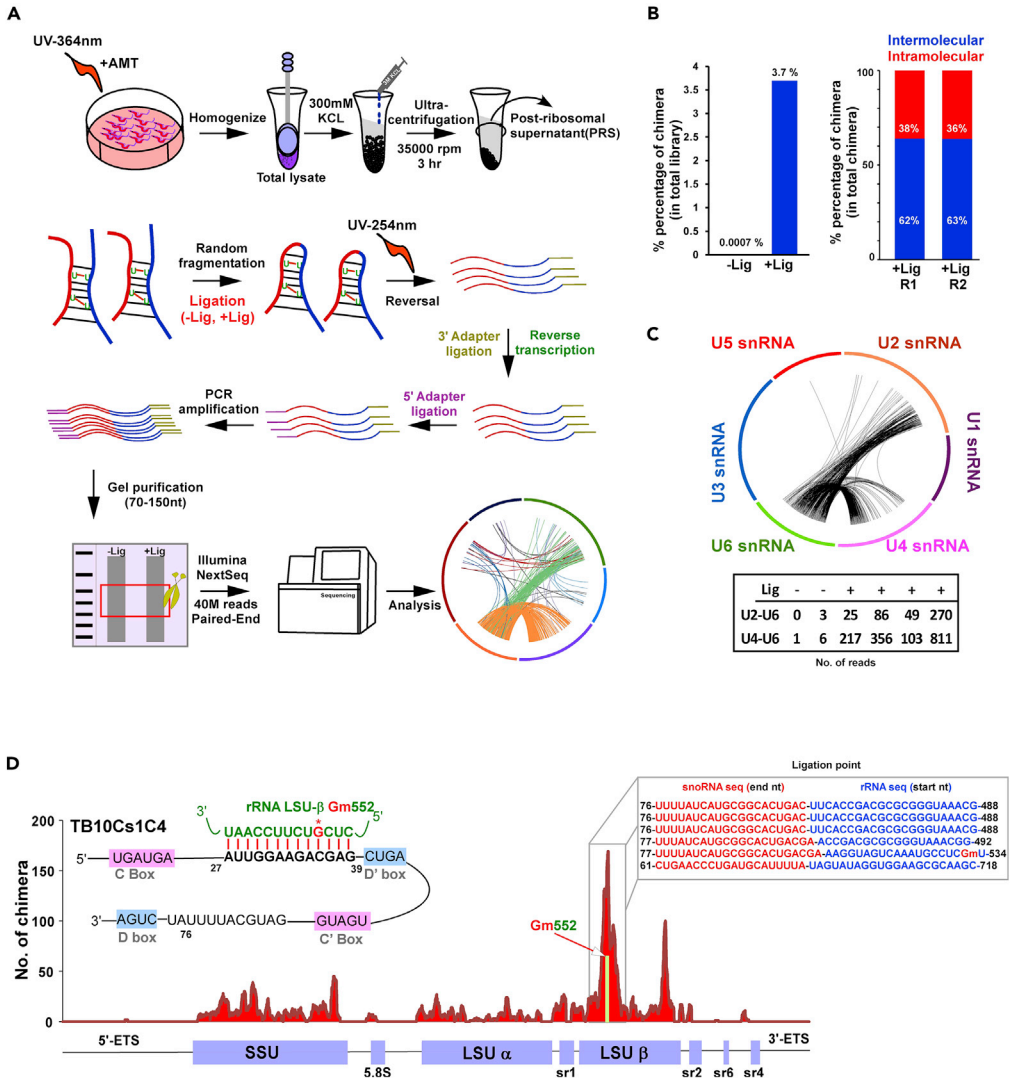

Figure 3. *T. brucei* ncRNA Interactome

(A) Schematic presentation of the ncRNA interactome identification protocol. The scheme illustrates the *in vivo* AMT-psoralen UV cross-linking treatment, extract preparation, fractionation, RNA extraction, mild fragmentation, ligation, and the RNA library preparation methodology.

(B) Enrichment of intermolecular RNA-RNA hybrids in ncRNA interactome upon ligation. The results show that the percentage of chimeric RNA increase from negligible to nearly 4% following ligation (left) and indicate the percentage of intermolecular cross-links in two replicates (right).

(C) Ciros plot representing the known interactions of U snRNA in *T. brucei* following ligation of cross-linked RNAs.

(D) Chimeric snoRNA-pre rRNA. The potential for base-pairing of TB10Cs1C4 with the pre-rRNA, and the coverage of ligation products between these RNAs in RPKM across the pre-rRNA are presented. An example of a chimeric RNA sequence and its target snoRNA is shown, demonstrating that ligation between the RNAs takes place close to the interaction domain. The different domains of the pre-rRNA are indicated.

enriched in the +ligation library compared to the –ligation library (Table S4, Data S4). The –ligation library can produce adducts resulting from ligation events that took place during library preparation, especially from strong base-pair interactions that were not dissociated during RNA extraction.

Analyzing the identity of the chimeric mRNAs that passed the above-mentioned criteria indicated that they belong mostly to mRNAs involved in metabolism and protein synthesis (Figure 4B). The Circos plot showed that ncRNAs interact with different mRNAs upon ligation (Figure 4C). The number of chimeric RNAs generated between the ncRNA and mRNA depends on the abundance of the ncRNA. For example, TBsRNA-32

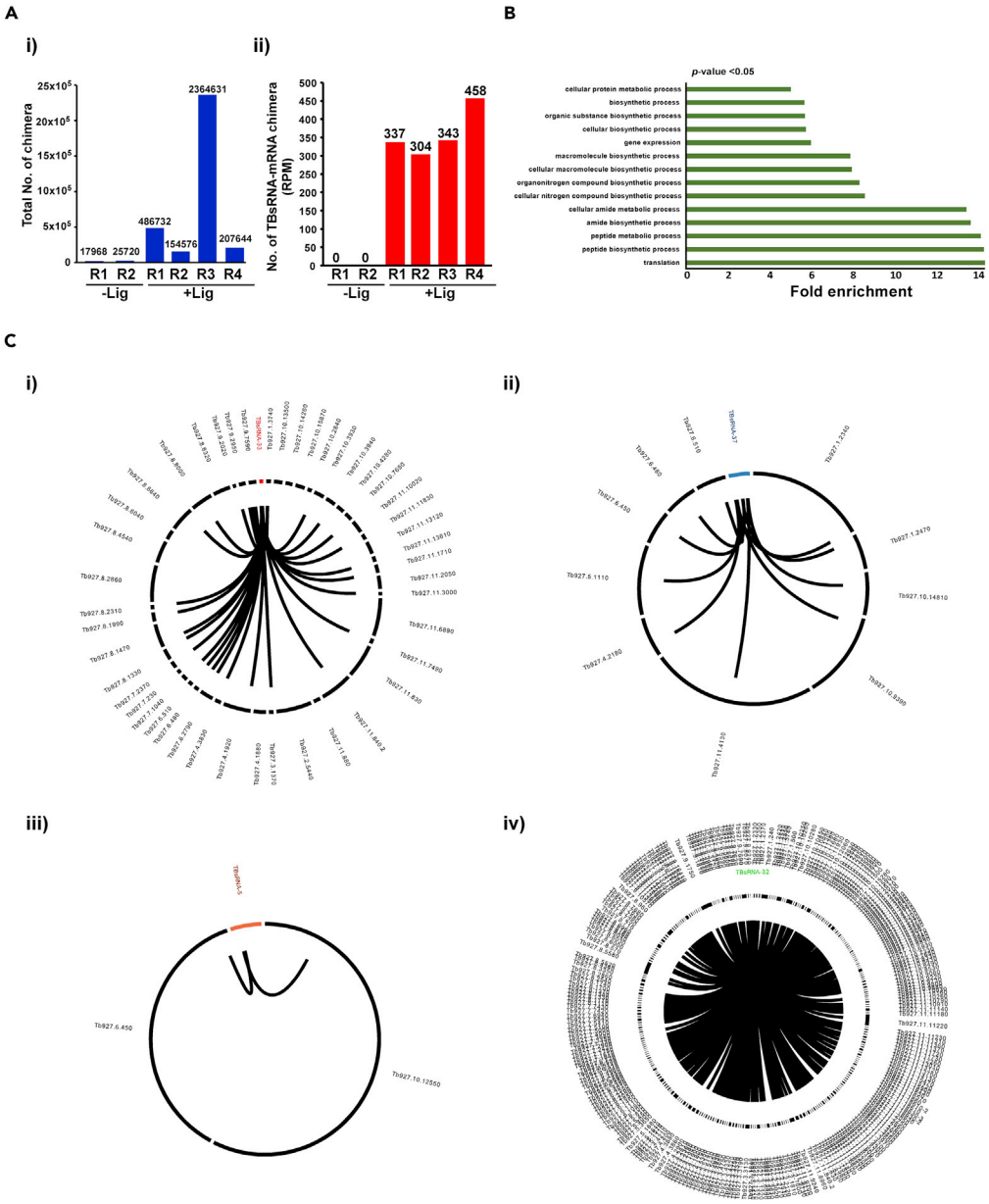

Figure 4. *T. brucei* TBsRNA Interactome

(A) (i) Enrichment of RNA-RNA hybrids in the ncRNA interactome upon ligation in various replicates. (ii) The total number of TBsRNA-mRNA chimeric reads obtained in each library.

(B) Gene ontology of mRNAs cross-linked with TBsRNA.

(C) Circos plots representing the interactions of TBsRNA with mRNAs in *T. brucei* upon ligation of cross-linked RNAs.

engages in numerous interactions, most likely because it is an abundant RNA in both life stages (Figure 4C). It is important to point out that we cannot rule out the possibility that our analysis missed additional interactions, especially with non-abundant mRNAs.

TBsRNA-33 Is an Anti-sense Repressor of Translation

To further study how these ncRNAs regulate their mRNA interaction partners, we chose to focus on TBsRNA-33. This ncRNA engages in cross-linking with ~14 mRNAs. Among these are six hypothetical proteins, two ribosomal proteins, and three proteins involved in protein modification (Table S5). Of special interest is the

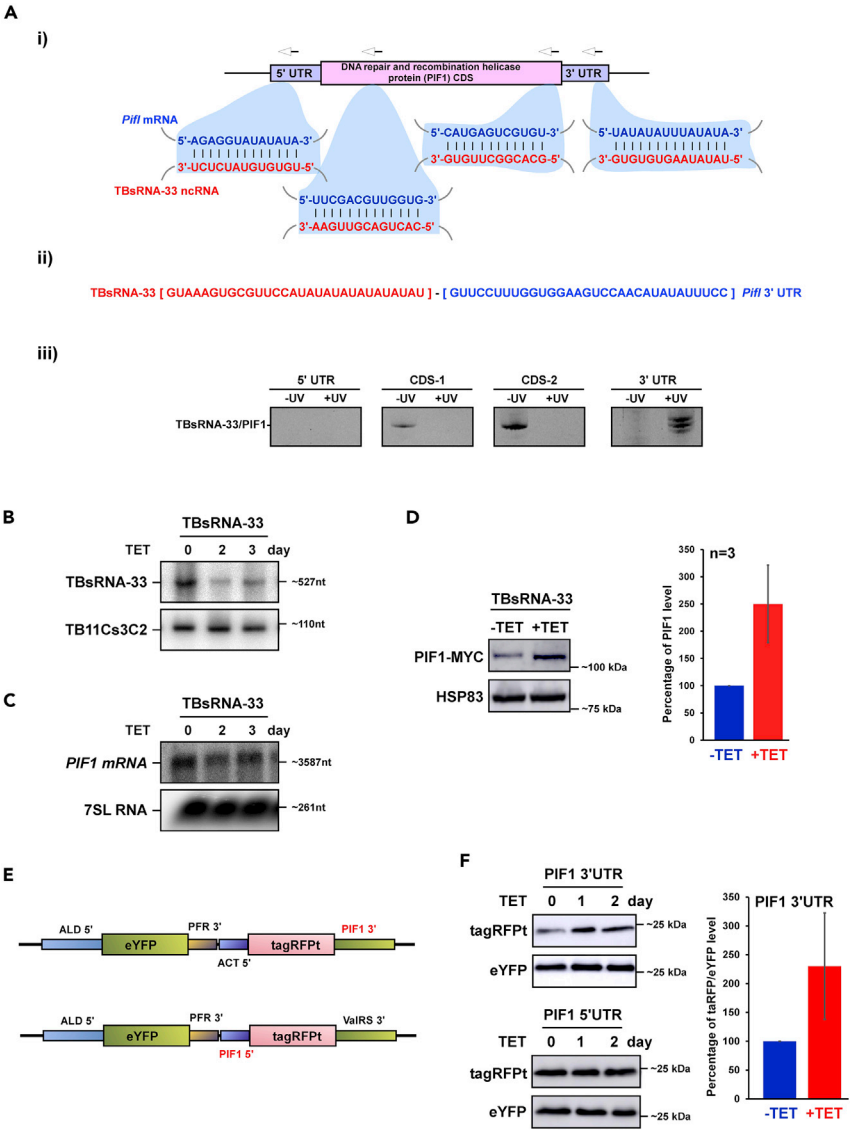

Figure 5. TBsRNA-33 Is an Anti-Sense Regulator of *T. brucei Pif1* mRNA

(A) TBsRNA-33 interacts with *Pif1* mRNA. (i) Schematic representation of the potential base-pairing between TBsRNA-33 and *Pif1* mRNA. The arrows indicated the positions of primers used in (iii) to amplify the chimeric RNA. (ii) The sequence of chimeric RNA formed by the interaction between TBsRNA-33 and *Pif1* mRNA 3′ UTR region is indicated from the PRS interactome library. (iii) Identification of TBsRNA-33 ligated to *Pif1* mRNA 3′ UTR by RT-PCR. Total RNA was prepared using the protocol described in (Figure 3A), and the cDNA was subjected to gene specific PCR using a forward primer from TBsRNA-33, and reverse primers corresponding to different regions of *Pif1* mRNA as indicated by the arrows in (i).

(B) TBsRNA-33 silencing. Cells carrying the silencing construct for TBsRNA-33 were silenced for the indicated days, and the RNA was subjected to Northern analysis with the indicated anti-sense probes.

(C) *Pif1* mRNA is not increased following TBsRNA-33 silencing. Total RNA (20 μg) was prepared from cells before and after TBsRNA-33 silencing, separated on a 1.2% agarose/formaldehyde gel and subjected to Northern analysis using RNA probes, as indicated. 7SL RNA served as a loading control.

(D) PIF1 translation is affected upon TBsRNA-33 silencing. PIF1 was tagged N-terminus with MYC tag in cells carrying the silencing construct for TBsRNA-33 and were silenced for the indicated days. Whole cell lysate from induced (+TET) and uninduced (-TET) was subjected to Western analysis with the indicated antibodies (left). The expression level for PIF1-MYC is presented as mean ± S.E.M (right). Experiments were done in triplicate (n = 3). The expression level of HSP83 was used as a loading control. All densitometry data used in this figure were calculated by ImageJ (https://imagej.nih.gov/ij/) software.

(E) Dicistronic reporter cassette containing PIF1 3′ or 5′ UTR. tagRFPt gene and PIF1 UTR was cloned in PPOTv4 vector carrying eYFP gene (Dean et al., 2015).

Figure 5. *Continued*

(F) TBsRNA-33 regulate PIF1 expression via its 3′ UTR. Dicistronic reporter cassette was introduced in cells carrying the silencing construct for TBsRNA-33 and were silenced for the indicated days. Whole cell lysate from induced (+TET) and uninduced (-TET) cells were subjected to Western analysis with the indicated antibodies (left). The expression level for tagRFPt is presented as mean ± S.E.M (right). Experiments were done in duplicate (n = 2). The expression level of eYFP was used as a loading control. All densitometry data used in this figure was calculated by ImageJ (https://imagej.nih.gov/ij/) software.

mRNA encoding for the DNA repair and recombination helicase protein, PIF1 encoded by Tb927.11.6890, which is essential because of its role in mitochondrial genome maintenance (Liu et al., 2010).

The potential of the ncRNA to interact with *Pif1* mRNA is presented in Figure 5Ai, indicating domains of possible interaction within the 5′ and-3′ UTR, and even within the open reading frame. To assess the validity of these interactions, the RNA from the cross-linking and ligation experiment, similar to the one presented in Figure 3A, was used to prepare cDNA, which was amplified with anti-sense primers to the *Pif1* mRNA depicted in Figure 5Ai, and sense primer from TBsRNA-33. The results provided evidence that TBsRNA-33 interacts by base-pairing via the 3′ UTR, as can also be seen by inspecting the sequencing of the chimeric molecule (Figures 5Aii and 5Aiii). Note that we also detected the chimeric molecule within the coding sequence (CDS) without UV cross-linking, probably because of strong interaction between TBsRNA-33 and *Pif1*mRNA CDS. The TBsRNA-33-*Pifl* chimera could not be detected in the poly (A) selected libraries, most likely because these mRNAs are associated with the mitochondrial ribosomes and could not be released without salt extraction. To determine how ncRNAs regulate mRNAs, the TBsRNA-33 was silenced by RNAi using a stem-loop construct (Kalidas et al., 2011). Silencing of the TBsRNA-33 ncRNA was confirmed by Northern analysis (Figure 5B). Next, we examined if silencing of TBsRNA-33 affects the expression of PIF1 protein. First, the level of *Pif1* mRNA was examined by Northern analysis over the course of the silencing, and no increase in the level of its mRNA was observed (Figure 5C). Next, the *Pif1* gene was tagged with MYC tag and the expression of the tagged protein was examined after silencing. The results indicate ∼2.5-fold increase in the level of the tagged PIF1 protein (n = 3), suggesting that TBsRNA-33 acts as an anti-sense repressor of PIF1 (Figure 5D). To explore the site of regulation by the ncRNA, the 5′ and 3′ UTRs of *Pif1* were cloned to flank the tagRFPt gene that is part of dicistronic cassette (Figure 5E). In this dicistronic cassette, the expression of tagRFPt changes as a result of 5′ or 3′ UTR composition, whereas eYFP serves as an internal control for expression. The results (Figure 5F) indicate that the regulation lies in the 3′ UTR of *Pif1*, supporting the potential interaction domain presented in (Figure 5A). The effect of silencing on cell viability (Figure 6A) showed a mild growth defect but increased sensitivity to pentamidine (Figure 6B) that is known to affect mitochondrial function (Gould and Schnaufer, 2014). The effect on mitochondria was further examined using tetramethyl rhodamine methylester (TMRM) which is a cationic lipophilic dye that enters cells and reversibly accumulates in the negatively charged mitochondrial matrix, depending on mitochondrial membrane potential (Goldshmidt et al., 2010). The silencing of TBsRNA-33 reduced the mitochondrial membrane potential ($\Delta\Psi$m) upon pentamidine treatment more than in control cells ($p < 0.014$) (Figure 6C), suggesting that this ncRNA modulates mitochondrial function (see below).

To examine if ncRNA level is changed under physiological conditions the level of eight ncRNAs were examined under heat-shock and starvation (Figures 6D, 6E, S3, and S4). The results showed that the level of several ncRNAs changed significantly ($p < 0.05$), under heat-shock of PCF at 41°C (Figures 6D and S3) or starvation for 1–3 hr (Figures 6E and S4). In particular, the level of TBsRNA-33 is reduced under both heat-shock and starvation. To examine if like silencing of TBsRNA-33 the level of PIF1 protein is increased, the level of the tagged PIF1 protein was examined following incubation at 41°C. Indeed, the level of MYC-tagged PIF1 protein was increased by ∼1.5 fold (n = 3) (Figure 6F), although the level of *Pif1* mRNA was reduced by ∼50% as the level of many mRNA under these conditions (Kramer et al., 2008) (Figure 6G).

This is a specific effect, since the level of MYC-tagged protein Enoyl-CoA hydratase/isomerase putative protein encoded by Tb927.11.10150, was reduced by 40% (Figure 6F) as was its mRNA (∼80% reduction) (Figure 6G). Based on these results, TBsRNA-33 is likely to function in repressing the translation of the *Pif1* mRNA, since when TBsRNA-33 levels were reduced, the level of MYC-tagged PIF1 protein increased. Interestingly, in BSF the level of TBsRNA-33 is increased by ∼2.7 fold (Figures 1F–1H) and *Pif1* mRNA is poorly translated (log2 (−1.78)) (Figure S5) (Jensen et al., 2014), suggesting that this ncRNA contribute to the regulation of mitochondrial mRNA translation in the two life stages of the parasite.

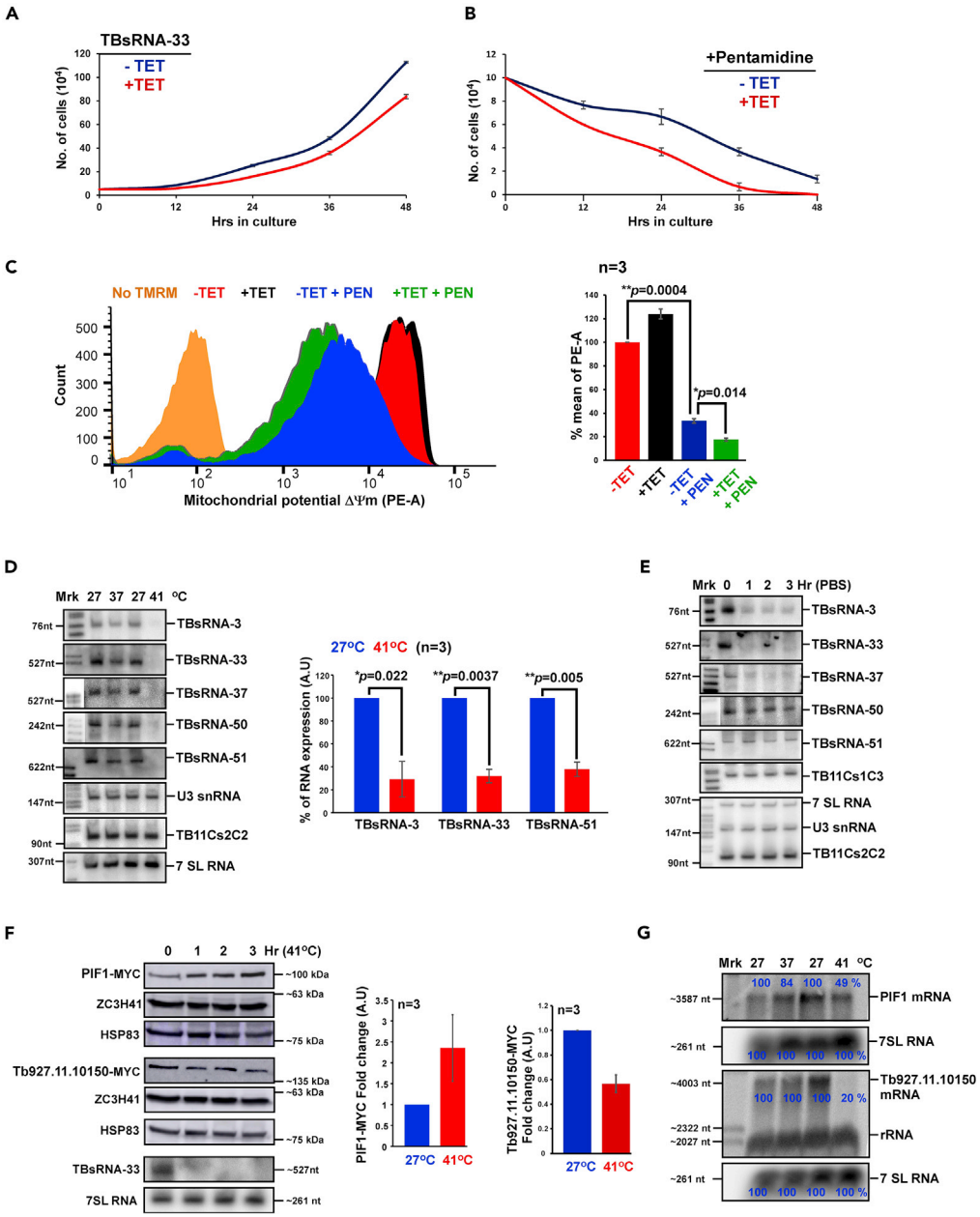

Figure 6. TBsRNA-33 Is an Anti-Sense Regulator of *T. brucei Pif1* mRNA

(A) Growth of cells upon TBsRNA-33 silencing. Uninduced cells carrying the silencing construct (-TET) were compared with cells induced for silencing (+TET) at 27°C. Data are presented as mean ± S.E.M. Experiments were done in triplicate (n = 3).

(B) Growth of cells upon TBsRNA-33 silencing and pentamidine treatment. Uninduced cells carrying the silencing construct (-TET) were compared with cells induced for silencing (+TET) upon treatment with 20μM pentamidine. Data are presented as mean ± S.E.M. Experiments were done in triplicate (n = 3).

(C). Silencing of TBsRNA-33 induces loss of mitochondrial membrane potential upon pentamidine treatment. Uninduced cells (-TET) and cells induced for silencing (+TET) upon treatment with 20μM pentamidine were harvested and treated with 150 nM TMRM in PBS with 0.2% glucose. The samples were incubated in the dark for 15 min at 27°C and then analyzed by FACS in PE channel. The cell count of cells with reduced $\Delta\Psi$m is plotted comparing the cells before and after two days of silencing. Data are presented as mean ± S.E.M (left). Experiments were done in triplicate (n = 3). Student's *t*-test was performed, and the p value is indicated.

(D) TBsRNAs are reduced upon heat-shock at 41°C. Total RNA (20 μg) from PCF cells subjected to heat-shock for 2 hr at the temperature indicated was separated on a 6% or 10% denaturing polyacrylamide gel and detected by Northern

Figure 6. *Continued*

analysis with ^{32}P-labeled anti-sense RNA probes to TBsRNA (left). The quantitative data derived from Northern analysis is presented as mean ± S.E.M (right). Experiments were done in triplicate (n = 3). Student's *t*-test was performed, and the p value is indicated. 7SL RNA was used as a loading control. ^{32}P-labeled pBR322 DNA *MspI* digest was used as a size marker.

(E) TBsRNAs are regulated upon starvation. Total RNA (20 μg) from PCF cells upon starvation in 1X PBS for the indicated time points was separated on 6% or 10% denaturing polyacrylamide gels and detected by Northern analysis.

(F) Western analysis of PIF1 protein following heat-shock. Total cell lysates were prepared from an equal number of cells before and after heat-shock and was subjected to western analysis using the indicated antibodies (left). The dilutions used for the antibodies are: (A) MYC (1:10,000), HSP83 (1:10,000), MTAP (1:10,000), and ZCH341 (1:10,000). The RNA derived from the same cells used for Western blot was subjected to Northern analysis. The data for PIF1-MYC is presented as mean ± S.E.M (right). Experiments were done in triplicate (n = 3). The expression level of HSP83 was used as a loading control.

(G) Northern analysis of *Pif1* mRNA following heat-shock. Total RNA (20 μg) was prepared under the conditions indicated, separated on a 1.2% agarose/formaldehyde gel and subjected to Northern analysis using RNA probes, as indicated. All densitometry data used in this figure was calculated by ImageJ (https://imagej.nih.gov/ij/) software

Next, the validity of interaction of TBsRNA-33 with rhodanese-like domain containing protein encoded by Tb927.11.13610 mRNA was examined (Table S5). The potential interaction domain of TBsRNA-33 with the Tb927.11.13610 mRNA target is presented (Figure 7A), and the chimera formed with the target mRNA is indicated (Figure 7B). The level of the Tb927.11.13610 mRNA was examined upon silencing of TBsRNA-33, and no change was observed (Figure 7C). To examine the possible effect on protein expression, the Tb927.11.13610 gene was tagged with the MYC tag, and its expression was examined. The results (Figures 7D and 7E) suggest that the level of rhodanese-like domain-containing protein was increased by ~1.7 fold upon silencing of TBsRNA-33 (n = 3), suggesting that similar to *Pif1* mRNA, the TBsRNA-33 serves as a translational repressor for Tb927.11.13610 mRNA.

TBsRNA-37 Is an Anti-sense Enhancer of Translation

TBsRNA-37 is encoded in the ITS7 of pre-rRNA (Figure 8A). Inspecting the RNA library of the chimeric RNA described above for interacting RNAs with TBsRNA-37 we identified four mRNAs, including the Macrocin-*O*-methyltransferase (TylF) encoded by Tb927.10.9390, which produces tylosin antibiotics active against gram positive bacteria (Seno and Baltz, 1981). The function of this protein is unknown in *T. brucei*. This chimera was detected in both PRS as well as poly(A) chimeric libraries. Moreover, this chimera was 3-fold enriched in the +ligation library. The potential for base-pairing between the ncRNA and its target mRNA is presented (Figure 8B). This potential interaction can also be seen by inspecting the sequencing of the chimeric molecule (Figure 8C). The ncRNA was silenced using a stem-loop RNAi construct and the RNA was subjected to Northern analysis showing efficient depletion (Figure 8D). Silencing was not associated with a growth defect under normal conditions (Figure 8E). No change in the level of *TylF* mRNA was observed upon silencing (Figure 8F). Next the *TylF* gene was tagged with MYC tag at the N-terminus and the expression was examined in the silenced cells, showing 50% reduction in the level of the protein ($p < 0.0013$) (Figure 8G), suggesting that this ncRNA enhances translation.

TBsRNA- 37 Interacts with the Ribosomes: A Model of Its Processing and Function

TBsRNA-37 is processed from ITS7 of its pre-rRNA (Figure 8A), but then moves to the cytoplasm, as it co-fractionates with the 80S ribosome. We therefore searched for its cross-linking with a mature rRNA sequence in the chimeric RNA library. TBsRNA-37 has the potential to base-pair with sr1 via 9 nts (Figure 9A), and indeed the majority of the chimeric reads are within the srRNA (sr1) (Figure 9B). Although we have no direct genetic evidence for the validity of such a base-pair interaction, there are no other possible interactions within sr1 apart from this proposed base-pairing. Whether the interaction with sr1 relies solely on base-pairing or also involves adapter protein(s) is currently unknown.

DISCUSSION

Anti-sense ncRNAs have been demonstrated to regulate gene expression in species ranging from bacteria to humans. These RNAs comprise small RNAs or long ncRNAs, as described above. Long ncRNAs were shown in trypanosomes to undergo *trans*-splicing and polyadenylation (Kolev et al., 2010). A few of these were shown to associate with ribosomes (Kolev et al., 2010). It was puzzling that neither long nor short anti-sense regulatory RNAs were described to date in trypanosomes, which appear to lack conventional micro-RNAs (Kolev et al., 2011). Here we focus on such ncRNA molecules that we show to regulate mRNA

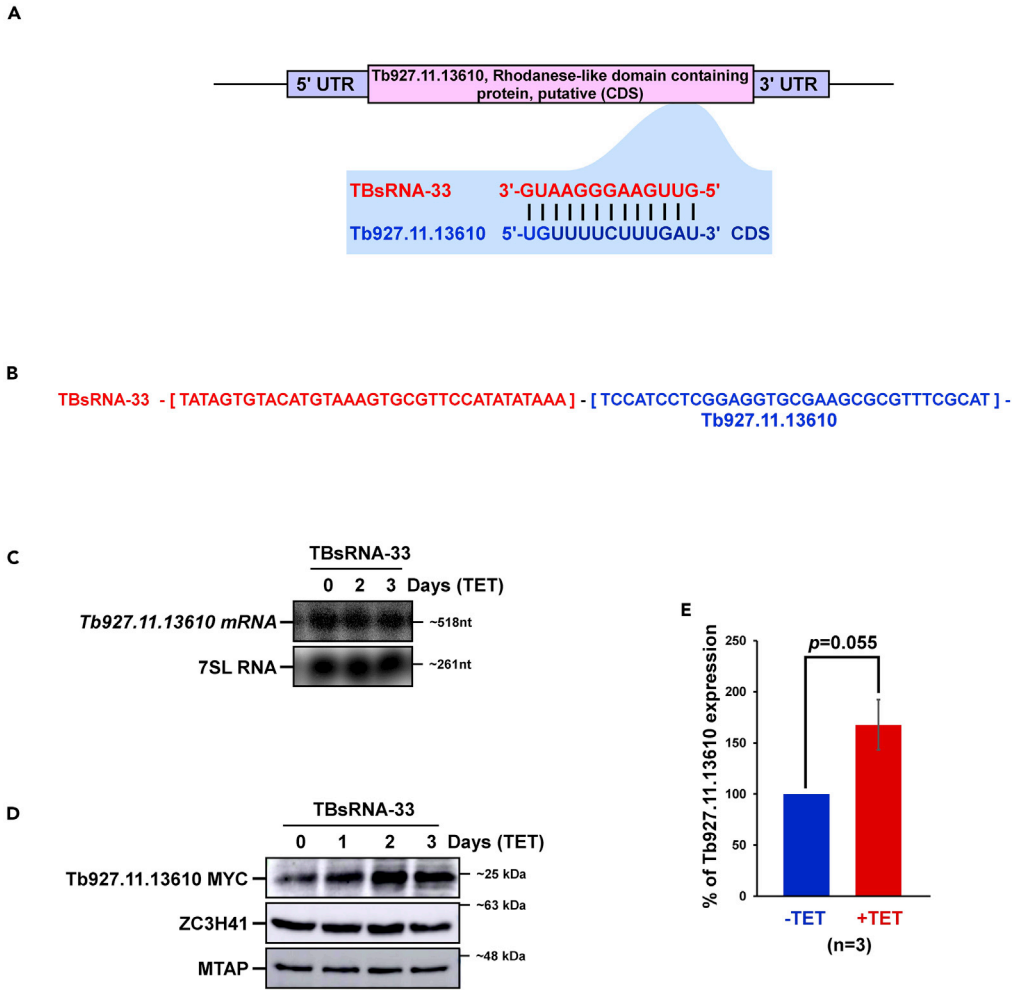

Figure 7. TBsRNA-33 Is an Anti-Sense Regulator of Tb927.11.13610, Rhodanese-like Domain-Containing Protein mRNA

(A) TBsRNA-33 interacts with Tb927.11.13610 mRNA. Schematic representation of the potential base-pairing between TBsRNA-33 and Tb927.11.13610 mRNA.

(B) The sequence of the chimeric RNA formed by the interaction between TBsRNA-33 and the Tb927.11.13610 CDS region is indicated based on the PRS interactome library.

(C) Tb927.11.13610 mRNA is not increased upon TBsRNA-33 silencing. Total RNA (20 μg) was prepared from cells before and after TBsRNA-33 silencing, separated on a 1.2% agarose/formaldehyde gel and subjected to Northern analysis using RNA probes, as indicated. 7SL RNA served as a loading control.

(D) Tb927.11.13610 translation is increased upon TBsRNA-33 silencing. Tb927.11.13610 was tagged with N-terminal MYC tag in cells carrying the silencing construct for TBsRNA-33 and were silenced for the indicated number of days. Whole cell lysates from induced (+TET) and uninduced (-TET) cultures were subjected to western analysis with the indicated antibodies (left). (E) The expression level for Tb927.11.13610-MYC is presented as the mean ± S.E.M. Experiments were performed in triplicate (n = 3). Student's *t*-test was calculated, and the p value is indicated. The expression level of HSP83 was used as a loading control. All densitometry data were calculated by ImageJ (https://imagej.nih.gov/ij/) software.

translation. Strikingly, RNAs TBsRNA-33 and 37 associates with the ribosome, have the potential to base-pair with rRNA, and do not exist as independent small RNA protein complexes like most known ncRNAs such as snoRNPs. We cannot exclude the possibility that these ncRNAs interact with ribosomal or other ribosome-associated protein(s).

Our study using deep sequencing of RNAs enriched in ribosome-free extracts revealed 62 novel ncRNAs and represents first steps in exploring this unique repertoire of novel ncRNAs. Of special interest are those

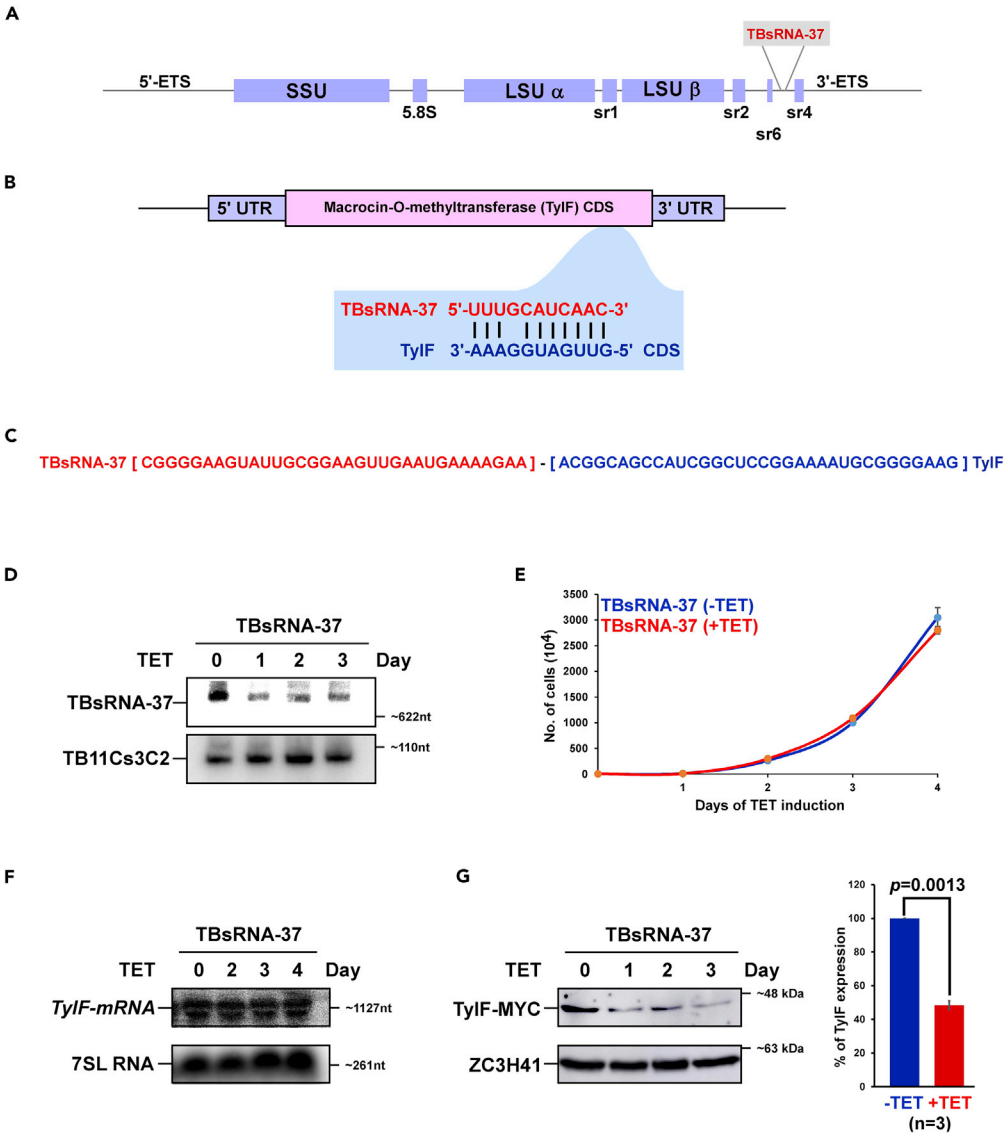

Figure 8. TBsRNA-37 Is an Anti-Sense Regulator of *TylF* mRNA

(A) TBsRNA-37 is encoded in the ITS7 of pre-rRNA. Schematic representation of the pre-rRNA locus from which TBsRNA-37 is derived is presented.

(B) TBsRNA-37 interacts with *TylF* mRNA. Schematic representation of the potential base-pairing between TBsRNA-37 and *TylF* mRNA.

(C) The sequence of chimeric RNA formed by the interaction between TBsRNA-37 and *TylF* mRNA CDS region is indicated based on the PRS interactome library.

(D) TBsRNA-37 silencing. Cells carrying the silencing construct for TBsRNA-37 were silenced for the indicated days, and the RNA was subjected to Northern analysis with the indicated anti-sense probes.

(E) Growth of cells upon TBsRNA-37 silencing. Uninduced cells carrying the silencing construct (-TET) were compared with cells induced for silencing (+TET) at 27°C. Data are presented as mean ± S.E.M. Experiments were done in triplicate (n = 3).

(F) *TylF* mRNA is not decreased upon TBsRNA-37 silencing. Total RNA (20 μg) was prepared from cells before and after TBsRNA-37 silencing, separated on a 1.2% agarose/formaldehyde gel, and subjected to Northern analysis using RNA probes, as indicated. 7SL RNA served as loading control. (G) TylF translation is reduced upon TBsRNA-37 silencing. *TylF* gene was tagged N-terminus with MYC tag in cells carrying the silencing construct for TBsRNA-37 and were silenced for the indicated days. Whole cell lysate from induced (+TET) and uninduced (-TET) was subjected to Western analysis with the indicated antibodies (left). The expression level for TylF-MYC is presented as mean ± S.E.M (right). Experiments were done in triplicate (n = 3). Student's *t*-test was performed, and the p value is indicated. The expression level of ZC3H41 was used as a loading control. All densitometry data used in this figure were calculated by ImageJ (https://imagej.nih.gov/ij/) software.

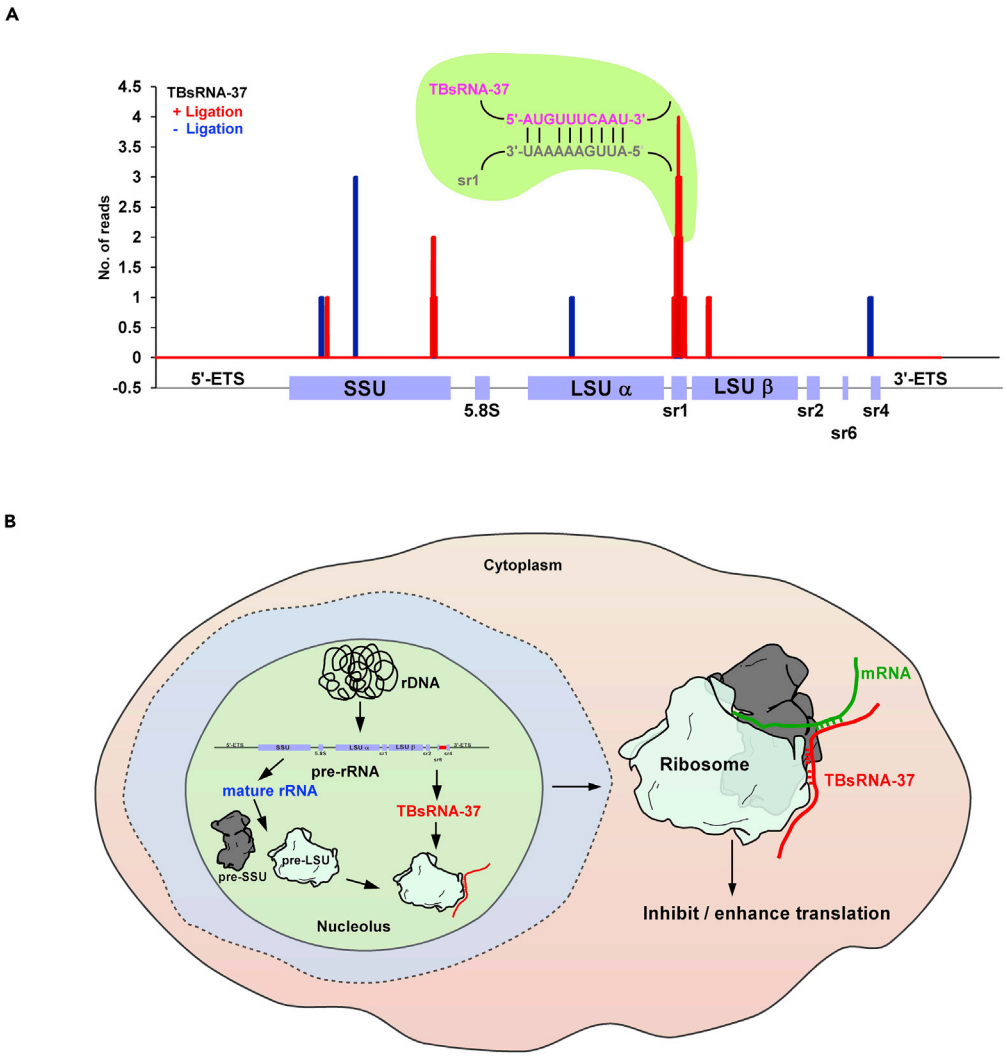

Figure 9. Proposed Model for the Mechanism of TBsRNA-37 as an Anti-Sense Regulator in *T. Brucei*

(A) TBsRNA-37 can potentially base-pair with mature rRNA. The coverage of ligation products of TBsRNA-37 across the pre-rRNA is shown from the PRS interactome library. The potential base-pairing of TBsRNA-37 with the srRNA-1 (sr1) is shown. The different domains of the pre-rRNA are indicated.

(B) The proposed mechanism for TBsRNA-37 interaction with its target mRNA. The ncRNA TBsRNA-37 is processed from the pre-rRNA in the nucleolus, potentially base-pairs with sr1 during the biogenesis of pre-LSU and moves together with the LSU to be assembled into a mature ribosome in the cytoplasm. In the cytoplasm, TBsRNA-37 remains base-paired with sr1 and interacts by base pairing to the target mRNA to inhibit or enhance translation.

ncRNAs that seem to interact mainly with ribosomes and potentially function as anti-sense regulators, as we show here for TBsRNA-33 and 37.

Among these new ncRNAs are stable RNAs that are processed from the spacers of pre-rRNA such as TBsRNA- 33, 50, 51 that are developmentally regulated and are highly expressed in BSF and their level is differentially regulated under starvation. Many of these ncRNAs listed above are likely to regulate the mRNAs they interact with. These ncRNA seem not to have a global effect on translation, but rather interact with only a small subset of mRNAs. Of special interest is TBsRNA-32 that becomes cross-linked to a variety of mRNAs. Although it is currently unknown how this RNA regulates their target mRNA. The ncRNAs can potentially either interact with 3′ UTR or 5′ UTR and affect stability and/or translation. We can also envision that like microRNAs these ncRNAs can affect the binding of an RBP (Kedde et al.,

2007). Differential binding of RBPs was shown to regulate both stability and translation of mRNA in a stage-dependent manner (Clayton, 2019). For instance, *T. brucei* hnRNPF/H stabilize or de-stabilize the same transcript in the two life stages of the parasite (Gupta et al., 2013b). This is the first study to highlight the presence of ncRNAs that are not derived from other stable RNAs but are generated to regulate the fate of specific mRNAs possibly by either repressing or enhancing stability and/or translation.

The study highlights the function of TBsRNA-33 and -37, which associate with the ribosome in the nucleolus, and likely move to the cytoplasm with the ribosome, where they affect the translation of a distinct set of mRNAs (Figure 9B). TBsRNA-33 is developmentally regulated, and its level is reduced under heat-shock and starvation. The genomic location of TBsRNA-33 and 37 is of special interest. It was previously reported that microRNAs can be processed from the rRNA ITS in *Drosophila* (Chak et al., 2015). However, here we report that the rDNA locus not only hosts ncRNAs that are processed from pre-rRNA spacers, but also ncRNAs that are transcribed from the anti-sense strand. In higher eukaryotes, microRNAs and snoRNAs are found in introns of pre-mRNA (Hesselberth, 2013). However, trypanosomes only possess two genes containing *cis*-spliced introns (Mair et al., 2000), which may explain why in trypanosomes, rDNA evolved to become the host of ncRNAs. Note that despite the length of all the TBsRNAs derived from pre-rRNA, which is similar to that of lncRNAs, we have no evidence for the presence of poly(A) at their 3′ end (Chikne et al., 2017) (Data S2). In addition, even the longer ncRNA among the 62 molecules described in this study, do not have significant potential for coding proteins or even small peptides (Table S5) (Kang et al., 2017).

Many of the ncRNAs listed in (Tables S1 and S2) are also highly expressed in the BSF. Since reduction in the level of TBsRNA-33 under heat-shock most likely relieves the inhibition on the translation of *Pif1* mRNA (Figure 4), we assume that the ncRNA acts as a repressor, and when its level is reduced during heat-shock, it can no longer repress the translation of its target mRNAs. Although the mechanism of action of TBsRNA-33 is currently unknown, RNA binding to a distinct site on the 3′ UTR can affect the binding of protein(s) that interact with the 43S initiation complex to enhance translation; alternatively the ncRNA may directly or via its binding protein inhibit translation, similar to the mechanism by which microRNAs arrest translation (Rissland, 2017). The mechanism of how TBsRNA-37 enhances translation of *TyIF* mRNA is currently unknown. The ncRNA can potentially bind a repressor that is bound to the target mRNA and by that relieve repression.

Based on the results obtained, we propose a model for the processing and function of TBsRNA-37 (Figure 9B). We suggest that the ncRNA is processed from pre-rRNA, potentially interacts with sr1, migrates with the ribosome to the cytoplasm, and during translation interacts with specific mRNAs. We currently do not know which protein(s) stabilize TBsRNA-33 and 37, but based on our RNA fractionation experiments, we favor the possibility that the RNA interacts directly with the ribosome and its association with the ribosome protects it from degradation. However, we cannot exclude the possibility that these ncRNA are bound during their biogenesis by protein(s) and that these are dislodged during fractionation. Half tRNA molecules were shown recently to associate with ribosomes in *T. brucei*. These are produced during nutrient deprivation and stimulate translation by facilitating mRNA loading during stress recovery, once starvation conditions are reversed (Fricker et al., 2019). However, the ncRNAs described here are not derived from stable RNAs.

Very little is known how the translation of proteins translocated to the mitochondria is regulated. Here we show that TBsRNA-33 regulates the translation of the *Pif1* mRNA that its protein is translocated to the mitochondria. We suggest a novel mechanism to regulate the mitochondria function in the two life stages of the parasite involving that action of anti-sense regulator. Since in BSF, the mitochondria is smaller and less active, therefore less of mitochondrial proteins should be translated. This is achieved by regulating the ncRNA that controls the translation of mitochondrial proteins in a stage-specific manner. TBsRNA-33 is highly expressed in BSF repressing the synthesis of the mitochondrial PIF1. Indeed, PIF1 is indeed essential for the mitochondrial function in PCF (Liu et al., 2010).

This study describes a novel mechanism to reduce or enhance translation via ncRNAs in *T. brucei*. This study presents the first report of a previously unknown level of regulation by ncRNAs and is likely only the tip of the iceberg in understanding the role of ncRNA is controlling gene expression during the cycling of the parasite between its hosts, or during its adaption to physiological cues such as heat-shock, starvation,

and oxidative stress during infection. Regulation by ncRNAs is quick and economical since it does not require additional synthesis of proteins to control gene expression under ambient conditions. Better understanding the mode of action of these novel ncRNAs can open the way to novel therapeutic approaches against these clinically significant parasites.

Limitations of the Study

The methodology used in this study to reveal ncRNA-target interaction using *in vivo* cross-linking and ligation of the interacting RNA molecules has limitations. The method requires a fragmentation step to enable ligation of the long target with the ncRNA. Mild fragmentation preserves the ncRNA but may not efficiently cleave longer RNA targets, thereby reducing the number of chimeric RNA molecules formed between the ncRNA and its target. Although most of the detected chimera were found in the interaction domain, other chimeric molecules were formed outside this domain, precluding the ability to unequivocally determine the exact base-pair interaction. The option of validating the interaction domain by mutating the interaction sequence or by introducing a compensatory mutation is not trivial for the ncRNA studied here because these originate from the rRNA locus.

The ultimate proof of our model for the function of TBsRNA-37 would be to find a tri-partite chimeric molecule that includes the ncRNA, the rRNA, and its mRNA target. However, for this RNA, we could not find such molecules, but were able to find examples of other mRNAs that are more abundant. Hence, the ability to find chimera from non-abundant RNAs (ncRNA or mRNA) is limited. Detection of the chimeric molecules varies between experiments and depends on efficiency of extraction of the RNPs (PRS extracts) and their associated RNAs.

Chimeric molecules were also detected in the non-ligated fraction because these could be formed between RNA molecules that are held together strongly by non-covalent interactions, or are very abundant in the pool and become ligated during the ligation step used for library preparation. Taking these limitations into account we focused on non-abundant mRNA targets that were at least 3-fold enriched in the ligation step performed before library preparation. In addition, we mainly considered the chimera that appeared in both types of RNA preparation (PRS and poly(A) selected RNA).

Resource Availability

Lead Contact

Further information and requests for resources and reagents should be directed to and will be fulfilled by the Lead Contact, Prof. Shulamit Michaeli (Shulamit.Michaeli@biu.ac.il).

Materials Availability

All plasmids, cell-lines, and in-house bioinformatics scripts used in this study are available on reasonable requests from the lead contact.

Data and Code Availability

The RNA sequencing data related to this study have been deposited in the NCBI Bioproject database under the accession number PRJNA630014. The data can be accessed using the following link: https://dataview.ncbi.nlm.nih.gov/object/PRJNA630014?reviewer=r8o4gaigdoao6t6nhitl1cku8k. Further information and requests for the bioinformatics codes used in this study should be directed to and will be fulfilled by the Lead Contact, Prof. Shulamit Michaeli (Shulamit.Michaeli@biu.ac.il).

METHODS

All methods can be found in the accompanying Transparent Methods supplemental file.

SUPPLEMENTAL INFORMATION

Supplemental Information can be found online at https://doi.org/10.1016/j.isci.2020.101780.

ACKNOWLEDGMENTS

This work was supported by a grant from the Israel-US Binational Science Foundation (BSF), and NIH grant R01 AI 056333 to C.T. S.M. holds the David and Inez Myers Chair in RNA silencing of diseases.

AUTHOR CONTRIBUTIONS

K.S.R: Methodology, visualization, formal analysis, and validation. K.S.R, B.G, S.A: Investigation, validation. S.C.C: Library preparation. K.S.R and T.G: Bioinformatics analysis. R.P: assistance in bioinformatics analysis. KSR, T.G, R.U, C.T, and S.M: Review and editing. R.U, C.T, and S.M: Funding acquisition and writing manuscript.

DECLARATION OF INTERESTS

The authors declare no competing financial interests.

Received: July 13, 2020
Revised: October 14, 2020
Accepted: November 3, 2020
Published: December 18, 2020

REFERENCES

Anders, S., and Huber, W. (2010). Differential expression analysis for sequence count data. Genome Biol. *11*, R106.

Barth, S., Hury, A., Liang, X., and Michaeli, S. (2005). Elucidating the role of H/ACA-like RNAs in trans -splicing and rRNA processing via RNA interference silencing of the trypanosoma brucei CBF5 pseudouridine synthase. J. Biol. Chem. *280*, 34558–34568.

Butter, F., Bucerius, F., Michel, M., Cicova, Z., Mann, M., and Janzen, C.J. (2013). Comparative proteomics of two life cycle stages of stable isotope-labeled trypanosoma brucei reveals novel components of the parasite's host adaptation machinery. Mol. Cell. Proteomics *12*, 172–179.

Chak, L.-L., Mohammed, J., Lai, E.C., Tucker-Kellogg, G., and Okamura, K. (2015). A deeply conserved, noncanonical miRNA hosted by ribosomal DNA. RNA *21*, 375–384.

Chikne, V., Doniger, T., Rajan, K.S., Bartok, O., Eliaz, D., Cohen-Chalamish, S., Tschudi, C., Unger, R., Hashem, Y., Kadener, S., and Michaeli, S. (2016). A pseudouridylation switch in rRNA is implicated in ribosome function during the life cycle of Trypanosoma brucei. Sci. Rep. *6*, 25296.

Chikne, V., Gupta, S.K., Doniger, T., K., S.R., Cohen-Chalamish, S., Waldman Ben-Asher, H., Kolet, L., Yahia, N.H., Unger, R., Ullu, E., et al. (2017). The canonical poly (A) polymerase PAP1 polyadenylates non-coding RNAs and is essential for snoRNA biogenesis in trypanosoma brucei. J. Mol. Biol. *429*, 3301–3318.

Chikne, V., Shanmugha Rajan, K., Shalev-Benami, M., Decker, K., Cohen-Chalamish, S., Madmoni, H., Biswas, V.K., Kumar Gupta, S., Doniger, T., Unger, R., et al. (2019). Small nucleolar RNAs controlling rRNA processing in Trypanosoma brucei. Nucleic Acids Res. *47*, 2609–2629.

Clayton, C. (2019). Regulation of gene expression in trypanosomatids: living with polycistronic transcription. Open Biol. *9*, 190072.

Clayton, C. (2013). The regulation of trypanosome gene expression by RNA-binding proteins. PLoS Pathog. *9*, e1003680.

Clayton, C.E. (2016). Gene expression in kinetoplastids. Curr. Opin. Microbiol. *32*, 46–51.

Dean, S., Sunter, J., Wheeler, R.J., Hodkinson, I., Gluenz, E., and Gull, K. (2015). A toolkit enabling efficient, scalable and reproducible gene tagging in trypanosomatids. Open Biol. *5*, 140197.

Fricker, R., Brogli, R., Luidalepp, H., Wyss, L., Fasnacht, M., Joss, O., Zywicki, M., Helm, M., Schneider, A., Cristodero, M., and Polacek, N. (2019). A tRNA half modulates translation as stress response in Trypanosoma brucei. Nat. Commun. *10*, 118.

Garrett-Wheeler, E., Lockard, R.E., and Kumar, A. (1984). Mapping of psoralen cross-linked nucleotides in RNA. Nucleic Acids Res. *12*, 3405–3424.

Goldshmidt, H., Matas, D., Kabi, A., Carmi, S., Hope, R., and Michaeli, S. (2010). Persistent ER stress induces the spliced leader RNA silencing pathway (SLS), leading to programmed cell death in trypanosoma brucei. PLoS Pathog. *6*, e1000731.

Gould, M.K., and Schnaufer, A. (2014). Independence from kinetoplast DNA maintenance and expression is associated with multidrug resistance in trypanosoma brucei in vitro. Antimicrob. Agents Chemother. *58*, 2925–2928.

Gupta, S.K., Hury, A., Ziporen, Y., Shi, H., Ullu, E., and Michaeli, S. (2010). Small nucleolar RNA interference in Trypanosoma brucei: mechanism and utilization for elucidating the function of snoRNAs. Nucleic Acids Res. *38*, 7236–7247.

Gupta, S.K., Kolet, L., Doniger, T., Biswas, V.K., Unger, R., Tzfati, Y., and Michaeli, S. (2013a). The Trypanosoma brucei telomerase RNA (TER) homologue binds core proteins of the C/D snoRNA family. FEBS Lett. *587*, 1399–1404.

Gupta, S.K., Kosti, I., Plaut, G., Pivko, A., Tkacz, I.D., Cohen-Chalamish, S., Biswas, D.K., Wachtel, C., Waldman Ben-Asher, H., Carmi, S., et al. (2013b). The hnRNP F/H homologue of Trypanosoma brucei is differentially expressed in the two life cycle stages of the parasite and regulates splicing and mRNA stability. Nucleic Acids Res. *41*, 6577–6594.

Hartshorne, T., and Agabian, N. (1993). RNA B is the major nucleolar trimethylguanosine-capped small nuclear RNA associated with fibrillarin and pre-rRNAs in Trypanosoma brucei. Mol. Cell Biol. *13*, 144–154.

Hesselberth, J.R. (2013). Lives that introns lead after splicing. Wiley Interdiscip. Rev. RNA *4*, 677–691.

Hombach, S., and Kretz, M. (2016). Non-coding RNAs: classification, biology and functioning. Adv. Exp. Med. Biol. *937*, 3–17.

Jensen, B.C., Ramasamy, G., Vasconcelos, E.J.R., Ingolia, N.T., Myler, P.J., and Parsons, M. (2014). Extensive stage-regulation of translation revealed by ribosome profiling of Trypanosoma brucei. BMC Genomics *15*, 911.

Kalidas, S., Li, Q., and Phillips, M.A. (2011). A Gateway® compatible vector for gene silencing in bloodstream form Trypanosoma brucei. Mol. Biochem. Parasitol. *178*, 51–55.

Kang, Y.-J., Yang, D.-C., Kong, L., Hou, M., Meng, Y.-Q., Wei, L., and Gao, G. (2017). CPC2: a fast and accurate coding potential calculator based on sequence intrinsic features. Nucleic Acids Res. *45*, W12–W16.

Kedde, M., Strasser, M.J., Boldajipour, B., Oude Vrielink, J.A.F., Slanchev, K., le Sage, C., Nagel, R., Voorhoeve, P.M., van Duijse, J., Ørom, U.A., et al. (2007). RNA-binding protein Dnd1 inhibits microRNA access to target mRNA. Cell *131*, 1273–1286.

Kolev, N.G., Franklin, J.B., Carmi, S., Shi, H., Michaeli, S., and Tschudi, C. (2010). The transcriptome of the human pathogen trypanosoma brucei at single-nucleotide resolution. PLoS Pathog. *6*, e1001090.

Kolev, N.G., Rajan, K.S., Tycowski, K.T., Toh, J.Y., Shi, H., Lei, Y., Michaeli, S., and Tschudi, C. (2019). The vault RNA of Trypanosoma brucei plays a role in the production of trans -spliced mRNA. J. Biol. Chem. *294*, 15559–15574.

Kolev, N.G., Ramey-Butler, K., Cross, G.A.M., Ullu, E., and Tschudi, C. (2012). Developmental progression to infectivity in Trypanosoma brucei triggered by an RNA-binding protein. Science *338*, 1352–1353.

Kolev, N.G., Tschudi, C., and Ullu, E. (2011). RNA interference in Protozoan parasites:

achievements and challenges. Eukaryot. Cell *10*, 1156–1163.

Kramer, S., Queiroz, R., Ellis, L., Webb, H., Hoheisel, J.D., Clayton, C., and Carrington, M. (2008). Heat shock causes a decrease in polysomes and the appearance of stress granules in trypanosomes independently of eIF2 phosphorylation at Thr169. J. Cell Sci. *121*, 3002–3014.

Liang, X.-H., Xu, Y.-X., and Michaeli, S. (2002). The spliced leader-associated RNA is a trypanosome-specific sn(o) RNA that has the potential to guide pseudouridine formation on the SL RNA. RNA *8*, S1355838202018290.

Liang, X., Haritan, A., Uliel, S., and Michaeli, S. (2003). Trans and cis splicing in trypanosomatids: mechanism, factors, and regulation. Eukaryot. Cell *2*, 830–840.

Liu, B., Yildirir, G., Wang, J., Tolun, G., Griffith, J.D., and Englund, P.T. (2010). TbPIF1, a trypanosoma brucei mitochondrial DNA helicase, is essential for kinetoplast minicircle replication. J. Biol. Chem. *285*, 7056–7066.

Mair, G., Shi, H., Li, H., Djikeng, A., Aviles, H.O., Bishop, J.R., Falcone, F.H., Gavrilescu, C., Montgomery, J.L., Santori, M.I., et al. (2000). A new twist in trypanosome RNA metabolism: cis-splicing of pre-mRNA. RNA *6*, 163–169.

Michaeli, S. (2014). Non-coding RNA and the complex regulation of the trypanosome life cycle. Curr. Opin. Microbiol. *20*, 146–152.

Michaeli, S. (2011). Trans-splicing in trypanosomes: machinery and its impact on the parasite transcriptome. Future Microbiol. *6*, 459–474.

Michaeli, S., Doniger, T., Gupta, S.K., Wurtzel, O., Romano, M., Visnovezky, D., Sorek, R., Unger, R., and Ullu, E. (2012). RNA-seq analysis of small RNPs in Trypanosoma brucei reveals a rich repertoire of non-coding RNAs. Nucleic Acids Res. *40*, 1282–1298.

Mohr, A.M., and Mott, J.L. (2015). Overview of microRNA biology. Semin. Liver Dis. *35*, 3–11.

Morris, K.V., and Mattick, J.S. (2014). The rise of regulatory RNA. Nat. Rev. Genet. *15*, 423–437.

Mugo, E., and Clayton, C. (2017). Expression of the RNA-binding protein RBP10 promotes the bloodstream-form differentiation state in Trypanosoma brucei. PLoS Pathog. *13*, e1006560.

Naguleswaran, A., Doiron, N., and Roditi, I. (2018). RNA-Seq analysis validates the use of culture-derived Trypanosoma brucei and provides new markers for mammalian and insect life-cycle stages. BMC Genomics *19*, 227.

Queiroz, R., Benz, C., Fellenberg, K., Hoheisel, J.D., and Clayton, C. (2009). Transcriptome analysis of differentiating trypanosomes reveals the existence of multiple post-transcriptional regulons. BMC Genomics *10*, 495.

Rajan, K.S., Chikne, V., Decker, K., Waldman Ben-Asher, H., and Michaeli, S. (2019a). Unique aspects of rRNA biogenesis in trypanosomatids. Trends Parasitol. *35*, 778–794.

Rajan, K.S., Doniger, T., Cohen-Chalamish, S., Chen, D., Semo, O., Aryal, S., Glick Saar, E., Chikne, V., Gerber, D., Unger, R., et al. (2019b). Pseudouridines on Trypanosoma brucei spliceosomal small nuclear RNAs and their implication for RNA and protein interactions. Nucleic Acids Res. *47*, 7633–7647.

Rajan, K.S., Zhu, Y., Adler, K., Doniger, T., Cohen-Chalamish, S., Srivastava, A., Shalev-Benami, M., Matzov, D., Unger, R., Tschudi, C., et al. (2020). The large repertoire of 2′-O-methylation guided by C/D snoRNAs on Trypanosoma brucei rRNA. RNA Biol. *17*, 1018–1039.

Rissland, O.S. (2017). The organization and regulation of mRNA-protein complexes. Wiley Interdiscip. Rev. RNA *8*, e1369.

Robinson, J.T., Thorvaldsdóttir, H., Winckler, W., Guttman, M., Lander, E.S., Getz, G., and Mesirov, J.P. (2011). Integrative genomics viewer. Nat. Biotechnol. *29*, 24–26.

Rodrigues, J.C.F., Godinho, J.L.P., and de Souza, W. (2014). Biology of human pathogenic trypanosomatids: epidemiology, lifecycle and ultrastructure. Subcell. Biochem. *74*, 1–42.

Sandhu, R., Sanford, S., Basu, S., Park, M., Pandya, U.M., Li, B., and Chakrabarti, K. (2013). A trans-spliced telomerase RNA dictates telomere synthesis in Trypanosoma brucei. Cell Res. *23*, 537–551.

Seno, E.T., and Baltz, R.H. (1981). Properties of S-adenosyl-L-methionine:macrocin O-methyltransferase in extracts of Streptomyces fradiae strains which produce normal or elevated levels of tylosin and in mutants blocked in specific O-methylations. Antimicrob. Agents Chemother. *20*, 370–377.

Tschudi, C., Shi, H., Franklin, J.B., and Ullu, E. (2012). Small interfering RNA-producing loci in the ancient parasitic eukaryote Trypanosoma brucei. BMC Genomics *13*, 427.

Wagner, E.G.H., and Romby, P. (2015). Small RNAs in bacteria and archaea: who they are, what they do, and how they do it. Adv. Genet. *90*, 133–208.

Wilson, R.C., and Doudna, J.A. (2013). Molecular mechanisms of RNA interference. Annu. Rev. Biophys. *42*, 217–239.

iScience, Volume *23*

Supplemental Information

Developmentally Regulated Novel Non-coding Anti-sense Regulators of mRNA Translation in *Trypanosoma brucei*

K. Shanmugha Rajan, Tirza Doniger, Smadar Cohen-Chalamish, Praveenkumar Rengaraj, Beathrice Galili, Saurav Aryal, Ron Unger, Christian Tschudi, and Shulamit Michaeli

Figure S1

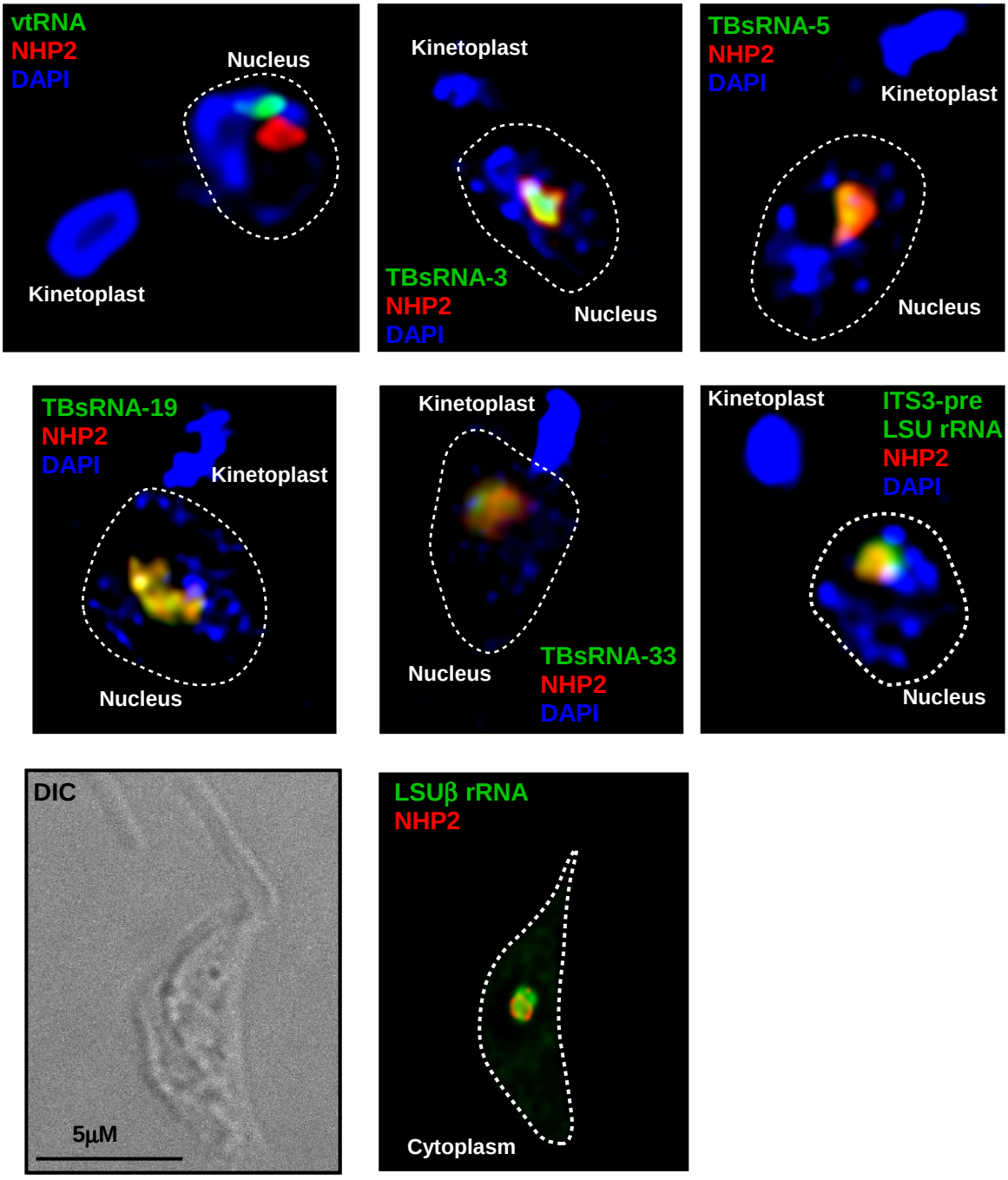
vtRNA
NHP2
DAPI
Nucleus
Kinetoplast
Kinetoplast
TBsRNA-3
NHP2
DAPI
Nucleus
TBsRNA-5
NHP2
DAPI
Kinetoplast
Nucleus
TBsRNA-19
NHP2
DAPI
Kinetoplast
Nucleus
Kinetoplast
Nucleus
TBsRNA-33
NHP2
DAPI
Kinetoplast
ITS3-pre
LSU rRNA
NHP2
DAPI
Nucleus
DIC
5µM
LSUβ rRNA
NHP2
Cytoplasm

Figure S1. High-resolution fluorescence *in situ* hybridization, Related to Figure 2. *in situ* hybridization coupled with immunofluorescence was performed for the indicated RNAs (green) and NHP2 (red). Nuclear and kinetoplast DNA was stained with DAPI (blue) and is indicated. The border of the nucleus is marked with dotted lines.

Figure S2

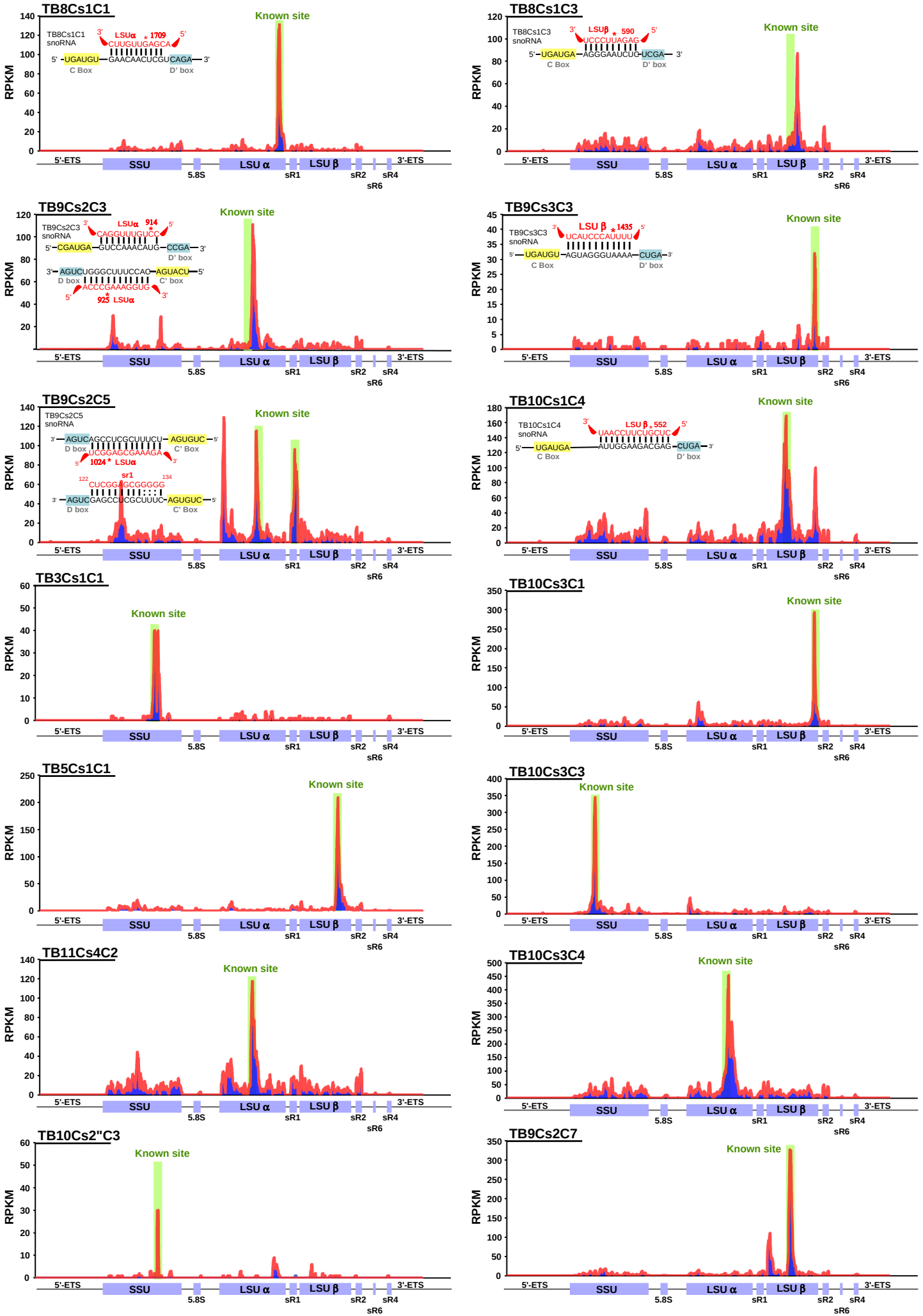
TB8Cs1C1
Known site
TB8Cs1C1 snoRNA
LSUα * 1709
CUUGUUGAGCA
5'-UGAUGU—GAACAACUCGU—CAGA-3'
C Box
D' box
TB8Cs1C3
Known site
TB8Cs1C3 snoRNA
LSUβ * 590
UCCCUUAGAG
5'-UGAUGA—AGGGAAUCUG—UCGA-3'
C Box
D' box
TB9Cs2C3
Known site
TB9Cs2C3 snoRNA
LSUα 914
CAGGUUUGUCC
5'-CGAUGA—GUCCAAACAUG—CCGA-3'
D' box
3'-AGUCUGGGCUUUCCAC—AGUACU-5'
D box
C' box
ACCCGAAAGGUG
925 LSUα
TB9Cs3C3
Known site
TB9Cs3C3 snoRNA
LSU β * 1435
UCAUCCCAUUUU
5'-UGAUGU—AGUAGGGUAAAA—CUGA-3'
C Box
D' box
TB9Cs2C5
Known site
TB9Cs2C5 snoRNA
3'-AGUCAGCCUCGCUUUCU—AGUGUC-5'
D box
C' Box
UCGGAGCGAAAGA
1024 * LSUα
sr1
122
CUCGGAGCGGGGGG
134
3'-AGUCGAGCCUCGCUUUC—AGUGUC-5'
D box
C' Box
TB10Cs1C4
Known site
TB10Cs1C4 snoRNA
LSU β * 552
UAACCUUCUGCUC
5'-UGAUGA—AUUGGAAGACGAG—CUGA-3'
C Box
D' box
TB3Cs1C1
Known site
TB10Cs3C1
Known site
TB5Cs1C1
Known site
TB10Cs3C3
Known site
TB11Cs4C2
Known site
TB10Cs3C4
Known site
TB10Cs2"C3
Known site
TB9Cs2C7
Known site
RPKM
5'-ETS
SSU
5.8S
LSU α
sR1
LSU β
sR2
sR4
sR6
3'-ETS

Figure S2. snoRNA-pre rRNA cross-linking ligation, Related to Figure 3. The coverage of ligated products between snoRNA and the rRNA across the pre-rRNA is shown. Data are presented as RPKM. The potential base-pairing of snoRNA with the pre-rRNA is indicated. The site of *2'O*-methylation on the rRNA is depicted. The different domains of the pre-rRNA are indicated.

Figure S3

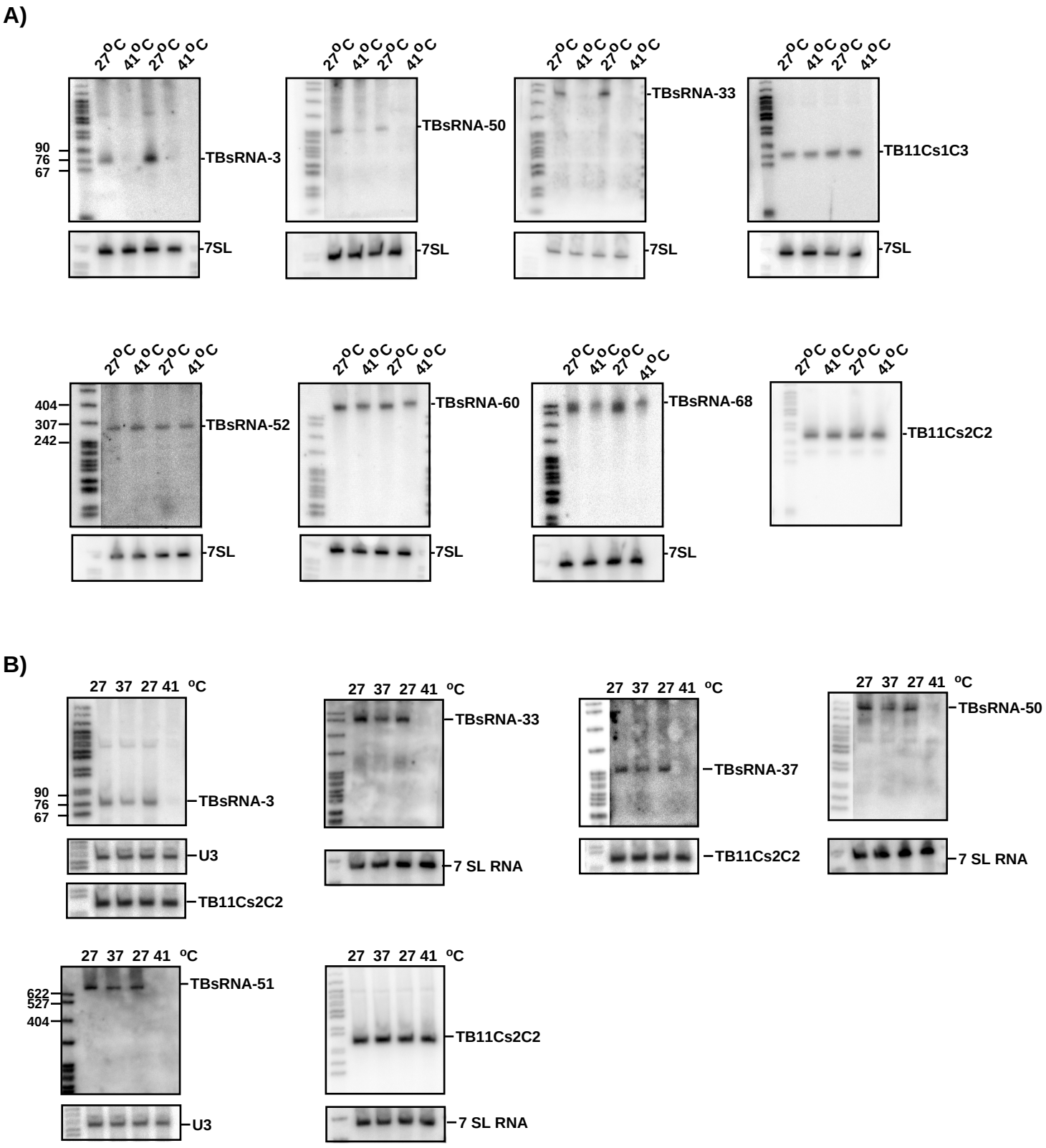
A)
27 °C 41 °C 27 °C 41 °C
90
76
67
TBsRNA-3
7SL
TBsRNA-50
TBsRNA-33
TB11Cs1C3
404
307
242
TBsRNA-52
TBsRNA-60
TBsRNA-68
TB11Cs2C2
B)
27 37 27 41 °C
TBsRNA-3
U3
TB11Cs2C2
TBsRNA-33
7 SL RNA
TBsRNA-37
TBsRNA-50
622
527
404
TBsRNA-51

Figure S3. Northern analysis, Related to Figure 6. A) Northern analysis demonstrating that TBsRNA are regulated upon heat-shock at 41ºC as shown in Figure 6D. Total RNA (20 μg) from two replicates of PCF cells upon heat-shock at 41ºC was separated on a 10% denaturing polyacrylamide gel and detected by Northern analysis with complementary probes to the specified TBsRNA. ^{32}P-labeled pBR322 DNA *MspI* digest was used as a size marker. **B)** Total RNA (20 μg) from PCF cells upon heat-shock, as indicated, was separated on 6% and 10% denaturing polyacrylamide gels, and detected by Northern analysis with complementary probes to the specified TBsRNA.

Figure S4

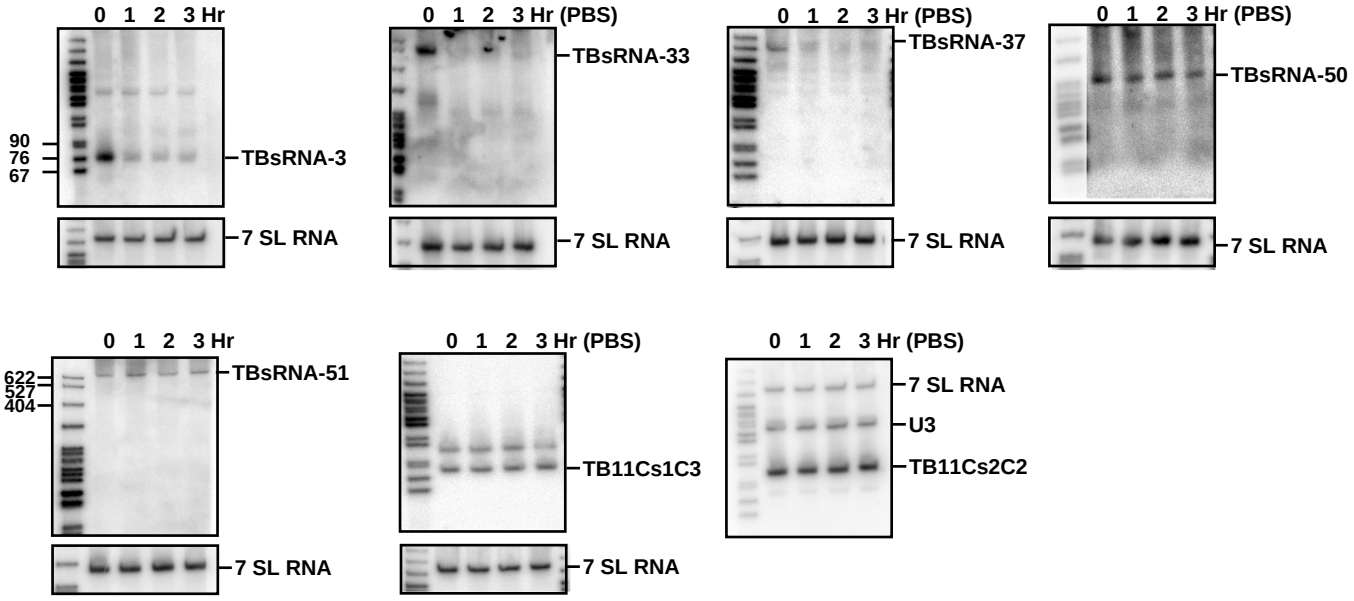
0 1 2 3 Hr
90
76
67
TBsRNA-3
7 SL RNA
0 1 2 3 Hr (PBS)
TBsRNA-33
7 SL RNA
0 1 2 3 Hr (PBS)
TBsRNA-37
7 SL RNA
0 1 2 3 Hr (PBS)
TBsRNA-50
7 SL RNA
0 1 2 3 Hr
622
527
404
TBsRNA-51
7 SL RNA
0 1 2 3 Hr (PBS)
TB11Cs1C3
7 SL RNA
0 1 2 3 Hr (PBS)
7 SL RNA
U3
TB11Cs2C2

Figure S4. Northern analysis, Related to Figure 6. Northern analysis demonstrating that TBsRNA are regulated upon starvation, as shown in Figure 6E. Total RNA (20 μg) from PCF cells upon starvation (incubation in PBS) for the indicated time, was separated on a 6% or 10% denaturing polyacrylamide gel and detected by Northern analysis with complementary probes to the specified TBsRNA. ^{32}P-labeled pBR322 DNA *MspI* digest was used as a size marker.

Figure S5

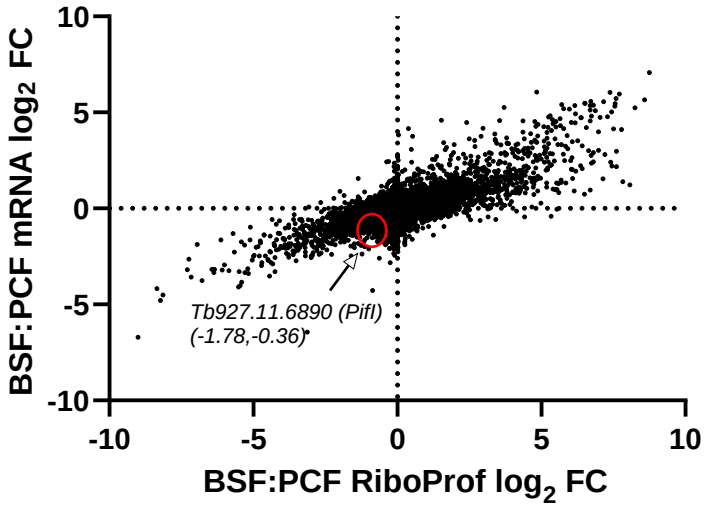
10
5
0
-5
-10
-10
-5
0
5
10
BSF:PCF mRNA log2 FC
BSF:PCF RiboProf log2 FC
Tb927.11.6890 (PifI)
(-1.78,-0.36)

Figure S5. *Pif1* mRNA is translated poorly in BSF, Related to Figure 5-6. Scatterplot highlighting the expression level of *Pif1* mRNA in the dataset of (Jensen et al., 2014). The data indicate log2 fold-change of mRNA abundance in the Y-axis and log2 fold-change of Ribosome profiling experiment in the X-axis. The RNA-seq data from BSF was compared against PCF. Indicated in dotted line are the four quadrants of the data.

Table S1. DESeq2 analysis of TBsRNAs in PRS RNA-seq libraries. The log2 fold-change (BSF vs PCF) and *p*-value is listed, Related to Figure 1.

TBsRNA	Log2 Fold-Change (BSF vs PCF)	*p-value*	*padj*
TBsRNA-1	3.6058	0.0001	0.0011
TBsRNA-11	2.7489	0.0017	0.0075
TBsRNA-12	3.8359	0.0036	0.0118
TBsRNA-14	-0.3721	0.5218	0.6006
TBsRNA-15	-2.3304	0.0007	0.0038
TBsRNA-16	-1.4538	0.0753	0.1350
TBsRNA-17	-1.5342	0.0649	0.1199
TBsRNA-18	-1.1902	0.1053	0.1785
TBsRNA-19	-1.3133	0.0309	0.0662
TBsRNA-2	2.5725	0.0018	0.0075
TBsRNA-20	0.2725	0.7494	0.7748
TBsRNA-22	-0.5354	0.4973	0.5833
TBsRNA-23	0.1420	0.8305	0.8443
TBsRNA-24	-0.0663	0.9117	0.9117
TBsRNA-29	-0.3636	0.6106	0.6897
TBsRNA-3	1.5655	0.0315	0.0662
TBsRNA-30	-1.2319	0.0814	0.1418
TBsRNA-31	-1.0160	0.1400	0.2173
TBsRNA-32	-1.4202	0.1397	0.2173
TBsRNA-33	3.9532	0.0037	0.0118
TBsRNA-34	1.8458	0.0223	0.0545
TBsRNA-35	0.7791	0.3001	0.3895
TBsRNA-37	2.8653	0.0157	0.0436
TBsRNA-38	3.8477	0.0200	0.0508
TBsRNA-39	-0.4897	0.6241	0.6907

TBsRNA-4	0.7943	0.1402	0.2173
TBsRNA-44	0.2250	0.7304	0.7681
TBsRNA-46	4.2850	0.0000	0.0000
TBsRNA-48	-3.6012	0.0000	0.0001
TBsRNA-49	1.2094	0.2771	0.3756
TBsRNA-5	-2.2730	0.0003	0.0017
TBsRNA-50	0.4501	0.4950	0.5833
TBsRNA-52	3.5979	0.0000	0.0001
TBsRNA-53	4.3822	0.0000	0.0000
TBsRNA-54	-1.5513	0.0474	0.0939
TBsRNA-55	-0.8956	0.2900	0.3846
TBsRNA-51	4.0695	0.0064	0.0187
TBsRNA-58	-0.9494	0.1902	0.2698
TBsRNA-59	2.3064	0.0064	0.0187
TBsRNA-6	0.5758	0.3227	0.4101
TBsRNA-60	-3.5370	0.0000	0.0001
TBsRNA-61	-0.3113	0.6341	0.6907
TBsRNA-62	-0.6593	0.4164	0.5080
TBsRNA-63	-0.7172	0.3438	0.4279
TBsRNA-64	1.8523	0.0020	0.0075
TBsRNA-65	1.0201	0.1425	0.2173
TBsRNA-66	-1.3328	0.0289	0.0653
TBsRNA-67	2.7756	0.0003	0.0017
TBsRNA-68	-1.8436	0.0165	0.0437
TBsRNA-69	-0.6882	0.1898	0.2698
TBsRNA-7	-2.0071	0.0021	0.0075
TBsRNA-70	0.8008	0.2644	0.3665
TBsRNA-72	3.2030	0.0000	0.0001
TBsRNA-73	0.9301	0.1715	0.2551
TBsRNA-74	1.4638	0.0537	0.1025
TBsRNA-75	2.4268	0.0003	0.0017

TBsRNA-76	0.1960	0.7229	0.7681
TBsRNA-77	-1.2722	0.0477	0.0939
TBsRNA-8	-1.9333	0.0014	0.0073
TBsRNA-9	1.8050	0.0260	0.0609

Table S2. The number of reads is presented for TBsRNA as reads per kilo-million (RPKM) from PRS RNA-seq libraries, Related to Figure 1.

TBsRNA	PCF1	PCF2	PCF3	BSF1	BSF2	BSF3
TBsRNA-1	28	30	104	23	181	224
TBsRNA-11	1016	1301	781	555	1819	1595
TBsRNA-12	2144	3022	2017	327	10540	2239
TBsRNA-14	182	101	208	85	11	59
TBsRNA-15	1080	1471	829	126	9	207
TBsRNA-16	3012	2389	2388	645	10	847
TBsRNA-17	5057	3661	2608	758	12	1294
TBsRNA-18	2174	2228	2687	609	28	1013
TBsRNA-19	2709	2663	2322	379	76	993
TBsRNA-2	599	732	468	332	886	1043
TBsRNA-20	215	36	133	17	36	34
TBsRNA-22	1585	606	625	581	9	298
TBsRNA-23	548	250	166	204	11	281
TBsRNA-24	753	308	359	179	22	431
TBsRNA-29	455	110	133	132	8	77
TBsRNA-3	1949	1517	995	3293	109	2977
TBsRNA-30	272	83	372	26	18	55
TBsRNA-31	681	298	1125	159	15	362
TBsRNA-32	34847	58905	40397	5797	867	19782
TBsRNA-33	5515	7808	2696	776	6605	2157
TBsRNA-34	35	91	46	41	55	28
TBsRNA-35	564	1916	1037	472	395	1059

TBsRNA-37	490	2074	377	458	2182	598
TBsRNA-38	141	85	212	2779	2	252
TBsRNA-4	500	282	280	354	57	292
TBsRNA-43	53	136	71	63	69	42
TBsRNA-47	0	0	0	0	3	1
TBsRNA-48	3155	304	2090	57	8	142
TBsRNA-5	777	1520	839	70	16	232
TBsRNA-50	1565	1169	969	999	159	406
TBsRNA-51	311	2638	1116	225	7682	654
TBsRNA-52	5	6	17	107	4	57
TBsRNA-53	1	2	2	8	5	21
TBsRNA-54	4071	1944	3129	843	20	649
TBsRNA-55	3105	2394	2710	1072	12	1250
TBsRNA-58	1971	1302	1294	510	20	647
TBsRNA-59	11	4	9	3	9	16
TBsRNA-6	413	429	249	147	94	259
TBsRNA-60	5778	3231	5942	152	17	502
TBsRNA-61	2500	2789	1548	982	210	870
TBsRNA-62	464	478	125	220	4	89
TBsRNA-63	2230	972	1053	553	30	611
TBsRNA-64	2	3	3	4	1	6
TBsRNA-65	75	28	42	18	19	41
TBsRNA-66	970	545	1048	156	16	331
TBsRNA-68	1361	1378	1716	272	8	383
TBsRNA-69	612	501	425	116	42	189
TBsRNA-7	1488	489	1034	166	10	162
TBsRNA-70	31	6	21	17	2	23
TBsRNA-72	3	2	3	4	6	8
TBsRNA-73	17	18	9	9	5	14
TBsRNA-74	143	39	141	286	10	103
TBsRNA-75	5	1	4	6	3	8

TBsRNA-76	73	35	78	34	9	31
TBsRNA-77	689	128	345	90	12	87
TBsRNA-8	782	179	515	65	8	94
TBsRNA-9	1700	1660	1383	517	1336	1751

Table S3. Distribution of chimeric RNA reads in different libraries, Related to Figure 3.

PRS interactome library

Sample	**Total no. of Sequences**	**Total no. of overlapping Sequences (after adapter/quality trimming)**	**Total no. of mapped sequences**	**Total no. of chimeric sequences**	**Total no. of Chimeric Sequences Pass Filter**
Minus UV Minus Ligation	49,241,940 X 2	43580939	37280375	41168	36358
Minus UV Plus Ligation	66,801,285 X 2	53304746	52556541	1790201	1525725
Minus UV Plus Ligation	41,835,021 X 2	35921911	33881009	861332	666266
Plus UV Minus Ligation	45,364,944 X 2	40512827	36269710	25795	21496
Plus UV Plus Ligation	100,778,254 X 2	87006242	86958177	3295684	2819898
Plus UV Plus Ligation	60,916,259 X 2	53057542	24143674	318511	250401

Poly (A) interactome library

Sample	Total no. of Sequences	Total no. of Sequences after trimming and filtering	Total no. of Chimeras	Total no. of Inter-Chimeras
Minus UV Plus Ligation Poly (A)	46,624,880 X 2	46,182,136 X 2	31,431,843	7,774,592
Minus UV Plus Ligation Poly (A)	37,879,253 X 2	37,584,041 X 2	27,416,010	6,877,177
Plus UV Plus Ligation Poly (A)	65,931,322 X 2	64,544,080 X 2	29,260,102	4,972,783
Plus UV Plus Ligation Poly (A)	49,085,110 X 2	48,081,098 X 2	23,406,540	4,486,831
Minus UV Minus Ligation Poly (A)	34,792,643 X 2	34,703,215 X 2	31,062,585	5,575,036
Minus UV Minus Ligation Poly (A)	35,813,140 X 2	35,718,575 X 2	31,649,871	5,871,618
Minus UV Minus Ligation Poly (A)	36,435,040 X 2	36,346,505 X 2	30,982,965	6,517,281

Table S4. List of potential TBsRNA-rRNA interaction, Related to Figure 3-4. Listed are those interactions enriched by more than 3 folds (log2 (1.58)) upon ligation. The Log2-Fold change of chimera sequence in plus ligation (LIGP) vs minus ligation (LIGM) and the normalized read counts in both PRS and poly (A) interactome libraries is indicated. Highlighted in green is the interaction of TBsRNA-37 with SrRNA1 (sr1) discussed in this study.

Interaction	Log2 _Fold-Change (LIGP Vs LIGM)	LIGM_PRS	LIGP_PRS	LIGM_Poly (A)	LIGP_Poly (A)
SSU+TBsRNA-9	4.44	0.00	6.49	0.00	11.84
SSU +TBsRNA-33	3.56	6.75	11.40	8.25	357.08
LSU_alpha+TBsRNA-33	3.35	0.00	5.09	13.75	230.82
SSU+TBsRNA-34	3.27	0.00	6.14	4.58	67.08
SSU+TBsRNA-55	3.17	0.00	17.02	1.83	11.84
sr2+TBsRNA-58	3.17	0.00	1.23	0.00	6.90

LSU_alpha+TBsRNA-34	3.01	0.00	1.93	1.83	46.36
sr2+TBsRNA-33	3.00	13.49	8.77	1581.82	110168.89
LSU_alpha+TBsRNA-36	2.91	0.00	1.75	0.92	25.65
sr4+TBsRNA-60	2.91	0.00	1.40	0.00	4.93
M5+TBsRNA-33	2.91	0.00	15.96	1.83	8.88
SSU+TBsRNA-42	2.86	0.00	5.44	0.00	1.97
SSU+TBsRNA-43	2.84	0.00	0.35	0.00	17.76
SSU+TBsRNA-51	2.68	0.00	4.91	19.26	161.77
LSU_alpha+TBsRNA-43	2.53	0.00	0.18	0.00	20.71
LSU_beta+TBsRNA-49	2.51	13.49	20.17	0.00	4.93
sr2+TBsRNA-51	2.36	0.00	0.18	0.00	15.78
LSU_alpha+TBsRNA-55	2.34	0.00	10.70	1.83	5.92
M5+TBsRNA-55	2.31	0.00	5.26	0.00	0.99
LSU_alpha+TBsRNA-8	2.30	0.00	1.05	0.00	2.96
M5+TBsRNA-48	2.29	0.00	5.09	0.00	0.99
SSU+TBsRNA-35	2.23	0.00	5.09	11.00	56.23
SSU+TBsRNA-37	2.23	0.00	2.46	2.75	23.67
sr4+TBsRNA-33	2.17	6.75	4.39	0.00	4.93
M5+TBsRNA-10	2.16	155.14	708.01	0.92	3.95
SSU+TBsRNA-10	2.13	364.24	868.88	11.00	89.76
Sr1+TBsRNA-37	2.12	0.00	2.11	0.92	8.88
sr4+TBsRNA-55	2.12	0.00	1.58	0.00	1.97
SSU+TBsRNA-12	2.04	0.00	27.02	41.26	59.18
sr4+TBsRNA-48	1.99	0.00	1.23	0.00	1.97
sr2+TBsRNA-10	1.98	134.90	161.74	0.92	16.77
SSU+TBsRNA-49	1.98	6.75	44.73	0.92	1.97
M5+TBsRNA-57	1.96	0.00	7.37	1.83	4.93

LSU_beta+TBsRNA-16	1.90	0.00	4.56	1.83	6.90
LSU_beta+TBsRNA-33	1.89	0.00	3.33	42.18	185.45
SSU+TBsRNA-39	1.88	0.00	3.86	0.92	3.95
sr2+TBsRNA-77	1.88	0.00	0.35	0.00	2.96
sr2+TBsRNA-24	1.87	0.00	0.18	0.00	5.92
Sr1+TBsRNA-35	1.86	0.00	10.17	4537.31	10554.65
LSU_beta+TBsRNA-10	1.85	242.83	642.23	11.92	59.18
SSU+TBsRNA-58	1.83	0.00	14.56	19.26	29.59
sr4+TBsRNA-10	1.76	87.69	389.62	0.92	1.97
SSU+TBsRNA-76	1.73	0.00	8.07	4.58	8.88
LSU_beta+TBsRNA-51	1.73	0.00	1.58	15.59	88.78
LSU_alpha+TBsRNA-77	1.71	0.00	1.23	1.83	14.80
Sr1+TBsRNA-33	1.69	13.49	8.07	4.58	68.06
SSU+TBsRNA-31	1.65	0.00	2.11	0.92	4.93
SSU+TBsRNA-36	1.64	6.75	2.81	3.67	51.29
M5+TBsRNA-54	1.64	0.00	1.93	0.00	0.99
Sr1+TBsRNA-51	1.62	0.00	3.51	11.00	35.51
sr2+TBsRNA-23	1.59	0.00	0.53	0.00	1.97

Table S5. mRNAs cross-linked with TBsRNA-33 only in the +ligation PRS interactome library, Related to Figure 3-4. Details regarding *Pif1* mRNA and rhodanese-like domain containing protein are highlighted in red.

Gene ID	**Product Description**
Tb927.4.1920	GPI transamidase subunit 16, putative
Tb927.7.2370	40S ribosomal protein S15, putative
Tb927.8.2860	hypothetical protein, conserved
Tb927.10.7650	hypothetical protein
Tb11.v5.0381	hypothetical protein, conserved
Tb927.11.18700	hypothetical protein, conserved
Tb927.11.19800	hypothetical protein
Tb927.11.1710	guide RNA-binding protein of 21 kDa
Tb927.11.2050	60S acidic ribosomal protein P0, putative
Tb927.11.6890	**DNA repair and recombination helicase protein PIF1**
Tb927.11.13120	PUB domain containing protein, putative
Tb927.11.13610	**rhodanese-like domain containing protein, putative**
Tb10.v4.0128	hypothetical protein

TRANSPARENT METHODS

Cell Growth

Procyclic *T. brucei* 427 (PCF) wild-type strain, and the genetically modified 29-13 strain, which carries integrated genes for T7 polymerase and the tetracycline repressor, were grown in SDM-79 medium supplemented with 10% fetal calf serum in the presence of 50 µg/ml hygromycin B and 15 µg/ml G418. The bloodstream form (BSF) of *T. brucei* strain 427, cell line 1313–514 (a gift from C. Clayton, ZMBH, Heidelberg, Germany) were aerobically cultivated at 37°C under 5% CO_2 in HMI-9 medium supplemented with 10% fetal calf serum, containing 2 µg ml^{-1} G418 and 2.5 µg ml^{-1} phleomycin (Chikne et al., 2016; Kolev et al., 2019; Michaeli et al., 2012; Rajan et al., 2020, 2019).

Northern analysis

RNAs were separated on a 6% or 10% (w/v) polyacrylamide gel containing 7 M urea or 1.2% agarose/formaldehyde gel and transferred onto nitrocellulose membranes. The RNA blots were hybridized to a ^{32}P labelled anti-sense RNA probe based on the primers listed in Supplementary Table T1 (Chikne et al., 2016; Kolev et al., 2019; Michaeli et al., 2012; Rajan et al., 2020, 2019).

RNA libraries from post-ribosomal supernatant (PRS)

Whole cell extracts were prepared from $5x10^9$ *T. brucei* PCF and BSF cells in a buffer containing 24mM KCL, 20mM Tris-pH7.8 and 10mM $MgCl_2$. RNPs were extracted using with 300mM KCL, and the ribosomes were removed by centrifugation for 3 hr at 35,000 rpm in a Beckman 70.1Ti rotor (150000 x g). The supernatant containing the post-ribosomal supernatant (PRS) was later deproteinized by digestion with proteinase K (Roche) (100 µg/ml in 1% SDS for 30 min at 37ºC), and RNA was prepared using TRIzol (Sigma) reagent. RNA extracted from the PRS was used for library preparation, essentially as described (Chikne et al., 2016; Rajan et al., 2019). The data analyzed in this study from the PRS was obtained from the libraries described in (Rajan et al., 2020, 2019)**.**

Identification of the ncRNA from RNA-seq.

First, the RNA-seq reads from each of the 15 PRS (9 procyclic and 6 bloodstream form) libraries (Rajan et al., 2020, 2019) were aligned to *T. brucei* v9 genome (https://tritrypdb.org/tritrypdb/). Using the tagBam program from the BEDTools suite v2.26.0 (Quinlan and Hall, 2010), we tagged all sequences belonging to known RNAs such as tRNA, rRNA, snoRNA, U snRNA, and mRNA. Then, alignments that remained untagged were converted into a BED file using the BEDTools "bamtobed" command. Overlapping entries in the BED file was then merged using the BEDTools "merge" command. The BEDTools "Multibamcov" program was then used to quantitate the expression of these regions.

In situ hybridization to localize the ncRNAs

Procyclic *T. brucei* cells were fixed on circular coverslips using 1.6% formaldehyde and permeabilized using Triton/Tween 20 (1:0.1%) in 1X PBS. *In situ* hybridization with specific DIG-labeled or CY3-labelled anti-sense RNA probes was performed as described (Kolev et al., 2019). The nucleolus was localized using anti-NHP2 antibody (0.7:1000 dilution) (Tkacz et al., 2008), and the nucleus was stained with 4,6-diamidino2-phenylindole (DAPI). Images were acquired using a Leica SP8 confocal microscope equipped with a white light laser and gating. Cells were oversampled both in the lateral and axial axis. The images were captured using a X100 HC Plan-Apo 1.4 NA objective at 512 X 512 pixels with Z slices taken every 200 nm. Excitation wavelengths used in this study were 405 nm for DAPI, 490 nm for detecting anti-DIG conjugated to FITC (hybrid detector at 496–552 nm with emission detection time gated 0.5–9.85 ns, and eight accumulations), and 552 nm for secondary anti-rabbit–Cy3 conjugated antibody. The images were then deconvolved using Huygens Professional software with standard parameters (SVI, Laapersveld 6, 1213 VB Hilversum, The Netherlands).

***In vivo* psoralen UV cross-linking and ligation to generate chimeric RNA.**

In vivo psoralen UV cross-linking was performed essentially as described in (Lustig et al., 2010; Rajan et al., 2019). Briefly, *T. brucei* cells were harvested and resuspended at 5×10^7 cells/ml and washed twice with PBS. Cells ($\sim5x10^9$) were concentrated and incubated on ice.

4′-Aminomethyltrioxsalen hydrochloride (AMT) (Sigma) was added to the cells at a concentration of 0.2 mg/ml for 30-40 minutes on ice. Cells treated with AMT were kept on ice and irradiated using a UV lamp at 365 nm, at a light intensity of 10 mW/cm^2 for 30 min. For PRS enriched with UV-crosslinked RNA, cells were washed once with PBS, and whole cell extracts were prepared from cells subjected to treatment with psoralen + UV crosslinking, and from samples not subjected to cross-linking in a buffer containing 24mM KCL, 10mM Tris-pH7.8 and 10mM $MgCl_2$. RNPs were extracted with 300mM KCL and the ribosomes were removed by centrifugation for 3 hr at 35,000 rpm in a Beckman 70.1Ti rotor (150000 x g). The supernatant was later deproteinized by digestion with proteinase K (Roche) (100 μg/ml in 1% SDS for 30 min) and RNA was prepared using TRIzol (Sigma) reagent. RNA extracted from the post-ribosomal supernatant (PRS) was used for library preparation, essentially as described below. For RNA enriched UV-crosslinked mRNA, poly (A) RNA was extracted using two rounds of oligo dT selection using the Dynabeads® mRNA DIRECT™ kit (Invitrogen), and libraries were prepared as below.

The cross-linked RNA was fragmented by mild alkaline hydrolysis using FastAP buffer (Thermo Scientific), dephosphorylated using FastAP Thermosensitive Alkaline Phosphatase (Thermo Scientific), cleaned by Agencourt RNA clean XP beads (Beckman Coulter), and the RNA-RNA hybrid was ligated using high concentration T4 RNA Ligase 1 (NEB) in a buffer containing DMSO, ATP, PEG 8000 and RNase inhibitor (NEB). The cross-linking between the ligated RNAs was reversed by irradiation at 254 nm. The recovered RNA was then used for library preparation, as previously described (Chikne et al., 2016; Rajan et al., 2020, 2019). Briefly, 800ng of PRS RNA was dephosphorylated with FastAP Thermosensitive Alkaline Phosphatase (Thermo Scientific), cleaned by Agencourt RNA clean XP beads (Beckman Coulter) and ligated to 3’ linker using high concentration T4 RNA Ligase 1 (NEB) in a buffer containing DMSO, ATP, PEG 8000 and RNase inhibitor (NEB). The ligated RNA-RNA hybrid was cleaned from excess linker using Dynabeads® MyOne™ SILANE beads (Thermo Scientific), and first strand cDNA was prepared using AffinityScript Reverse Transcriptase (Agilent). The RNA was subsequently degraded using 2□l of 1M NaOH, and the cDNA was cleaned using Dynabeads® MyOne™ SILANE beads (Thermo Scientific). The cDNA was further ligated to 3’ adapter using high concentration T4 RNA Ligase 1 (NEB) and cleaned of excess adapter by using Dynabeads® MyOne™ SILANE beads (Thermo Scientific). The adapter ligated cDNA was PCR enriched using NEBNext® High-Fidelity (NEB) polymerase

(9 PCR cycles), separated on an E-Gel EX agarose gel (Invitrogen) and size selected in the range of 150-300 bp (containing ~30-180nt corresponding to the input RNA). The amplicons were gel purified using NucleoSpin Gel and PCR Clean-up kit (Macherey-Nagel) and sequenced in a NextSeq system (Illumina) in paired end mode (20-40 million reads for each sample).

Analysis of chimeric RNA

The reads from the RNA-seq as described above were preprocessed using Trim Galore v0.5.0 (https://www.bioinformatics.babraham.ac.uk/projects/trim_galore/). Overlapping read pairs were merged using FLASH v1.2.11 (Magoc and Salzberg, 2011). BWA-MEM v0.7.17-r1188 (Li and Durbin, 2009) was used to align the reads to a custom made *T. brucei* transcriptome database. The SAM output was converted to BAM using SAMTools. The scripts from the SPLASH computational pipeline (Aw et al., 2016) were used to identify the chimeric RNA from the BAM files. The "find_chimeras.py" script was used to detect chimeric RNA. In the case of "intramolecular" chimeric RNA, the ligated RNAs were required to be spaced at least a 15 nts apart in the same transcript. Circos program (Krzywinski et al., 2009) was used to generate the plots illustrating the interacting chimeric RNAs.

N-terminal MYC Tagging

N-terminal MYC tagged Tb927.11.6890 (PIF1), Tb927.10.9390 (TyIF), Tb927.11.13610 and Tb927.11.10150 constructs were prepared by cloning ~500nt of the respective sequences into pNAT X-tag (a gift from Dr. Sam Alsford, London School of Hygiene & Tropical Medicine, UK). The primers used are listed in Supplementary Table T1. The plasmids were linearized with *BsrGI, ClaI, BstBI* and *AvaI*, respectively for integration into the authentic chromosomal loci.

Dicistronic reporter cassette

To create a dicistronic reporter cassette, the tagRFPt gene was first cloned into PPOTv4 vector (a gift from Dr. Samuel Dean, Sir William Dunn School of Pathology, University of Oxford, UK) carrying eYFP and blasticidin resistance gene (Dean et al., 2015) between the *NheI* and *XhoI* restriction site. This vector was further used to clone PIF1 3' UTR between *XhoI* and *NsiI*

restriction site, whereas PIF1 5' UTR was cloned between *SphI* and *NheI* restriction site. The resulting construct was linearized with *BsaBI* enzyme for integration into the PFR2 locus.

SUPPLEMENTARY REFERENCES

Aw, J.G.A., Shen, Y., Wilm, A., Sun, M., Lim, X.N., Boon, K.-L., Tapsin, S., Chan, Y.-S., Tan, C.-P., Sim, A.Y.L., Zhang, T., Susanto, T.T., Fu, Z., Nagarajan, N., Wan, Y., 2016. In Vivo Mapping of Eukaryotic RNA Interactomes Reveals Principles of Higher-Order Organization and Regulation. Mol. Cell 62, 603–617.

Chikne, V., Doniger, T., Rajan, K.S., Bartok, O., Eliaz, D., Cohen-Chalamish, S., Tschudi, C., Unger, R., Hashem, Y., Kadener, S., Michaeli, S., 2016. A pseudouridylation switch in rRNA is implicated in ribosome function during the life cycle of Trypanosoma brucei. Sci. Rep. 6, 25296.

Dean, S., Sunter, J., Wheeler, R.J., Hodkinson, I., Gluenz, E., Gull, K., 2015. A toolkit enabling efficient, scalable and reproducible gene tagging in trypanosomatids. Open Biol. 5, 140197.

Jensen, B.C., Ramasamy, G., Vasconcelos, E.J.R., Ingolia, N.T., Myler, P.J., Parsons, M., 2014. Extensive stage-regulation of translation revealed by ribosome profiling of Trypanosoma brucei. BMC Genomics 15, 911.

Kolev, N.G., Rajan, K.S., Tycowski, K.T., Toh, J.Y., Shi, H., Lei, Y., Michaeli, S., Tschudi, C., 2019. The vault RNA of Trypanosoma brucei plays a role in the production of trans - spliced mRNA. J. Biol. Chem. 294, 15559–15574.

Krzywinski, M., Schein, J., Birol, I., Connors, J., Gascoyne, R., Horsman, D., Jones, S.J., Marra, M.A., 2009. Circos: an information aesthetic for comparative genomics. Genome Res. 19, 1639–45.

Li, H., Durbin, R., 2009. Fast and accurate short read alignment with Burrows-Wheeler transform. Bioinformatics 25, 1754–1760.

Lustig, Y., Wachtel, C., Safro, M., Liu, L., Michaeli, S., 2010. 'RNA walk' a novel approach to study RNA–RNA interactions between a small RNA and its target. Nucleic Acids Res. 38, e5–e5.

Magoc, T., Salzberg, S.L., 2011. FLASH: fast length adjustment of short reads to improve genome assemblies. Bioinformatics 27, 2957–2963.

Michaeli, S., Doniger, T., Gupta, S.K., Wurtzel, O., Romano, M., Visnovezky, D., Sorek, R., Unger, R., Ullu, E., 2012. RNA-seq analysis of small RNPs in Trypanosoma brucei reveals a rich repertoire of non-coding RNAs. Nucleic Acids Res. 40, 1282–1298.

Quinlan, A.R., Hall, I.M., 2010. BEDTools: a flexible suite of utilities for comparing genomic features. Bioinformatics 26, 841–842.

Rajan, K.S., Doniger, T., Cohen-Chalamish, S., Chen, D., Semo, O., Aryal, S., Glick Saar, E., Chikne, V., Gerber, D., Unger, R., Tschudi, C., Michaeli, S., 2019. Pseudouridines on Trypanosoma brucei spliceosomal small nuclear RNAs and their implication for RNA and protein interactions. Nucleic Acids Res. 47, 7633–7647.

Rajan, K.S., Zhu, Y., Adler, K., Doniger, T., Cohen-Chalamish, S., Srivastava, A., Shalev-Benami, M., Matzov, D., Unger, R., Tschudi, C., Günzl, A., Carmichael, G.G., Michaeli, S., 2020. The large repertoire of 2'-O-methylation guided by C/D snoRNAs on Trypanosoma brucei rRNA. RNA Biol. 1–22.

Tkacz, I.D., Cohen, S., Salmon-Divon, M., Michaeli, S., 2008. Identification of the heptameric Lsm complex that binds U6 snRNA in Trypanosoma brucei. Mol. Biochem. Parasitol. 160, 22–31.